Dalton Transactions

Accepted Manuscript

ROYAL SOCIETY OF CHEMISTRY

www.rsc.org/dalton

Dec 31, 2014

To
The Editor
Dalton Transactions

Ref: DT-ART-11-2014-003429

"Homodinuclear Lanthanide {Ln2} (Ln = Gd, Tb, Dy, Eu) Complexes Prepared from o-Vanillin based Ligand: Luminescence and Single-Molecule Magnetism Behavior."

Dear Editor:
Please find enclosed the revised version of the above manuscript. The entire revised portion has been highlighted (yellow color) in the manuscript as well as in the SI.

The following is the detailed response to the referee queries:

Referee: 1

Comments to the Author
This manuscript describes the synthesis, structures, luminescent and magnetic properties of four dinuclear lanthanide complexes. Although the structure of the ligand is not novel, and the structures of the complexes are not aesthetically pleasing, the complexes exhibit strong ligand-sensitized lanthanide-characteristic emission. The complex 2 shows a very high overall quantum yield. Complex 3 displays single-molecule magnet behavior and shows a two-step slow relaxation. I recommend for the acceptable of the manuscript after minor revision.

(1) The magnetic properties of complex 4 are not investigated. Why?

Response: Because the typical nonmagnetic ground state (7F0) is expected for europium analog at low temperatures and due to the presence of thermally populated excited states, the magnetic properties of such compounds remain difficult to interpret even at room temperature.

(2) The IR spectra of the complexes should be provided in the Supporting Information.

Response: Now, we have provided IR spectra of all the four compounds in the ESI (Figs. S20-S23)

(3) As the solvent CHCl3 was determined, the TD-DTG spectra should be provided. XRD of the complexes should be determined.

Response: Now we have provided PXRD of compounds 1-3 as these complexes were used for magnetic measurementsESI (Fig 24-26). TGA graphs are now included for 1-4 in the ESI (Fig. S27).
We have also included text regarding these measurements in the manuscript.

(4) The formats of the Tables should be re-edited.

Response: Now we have reedited the tables in SI

(5) Some small errors should be corrected. e.g. (H3L) in Abstract should not be bold. LH3 in the text [(H2L)4Ln2(piv)4] Figures 1 and 3.
Lanthanide-centerd found to be to be above data suggests to its triplet state (S1-T1) iii) triplet state energy level (1ðð*) and the triplet energy (3ðð*) level of the ligand was transfer process in complexes 2-4. 1-3 or 2-4 ? 1-3) in the temperature range at 1-1500 Hz (Fig. 11). Fig 11 is only for complex 3 {LH2]-

Response: Thanks a lot, for pointing out these mistakes. These have been corrected.

Referee: 2

Comments to the Author

The manuscript details the synthesis of a family of dinuclear lanthanide complexes, with subsequent analysis of the physical (photo and magnetic) properties. I am satisfied by the originality of the work, using the ligand 2,2'-(2-hydroxy-3-methoxy-5-methylbenzylazanediyl)diethanol and Ln(III) ions to display SMM behaviour and luminescence in the same complex. I feel this work is therefore of importance to the wider inorganic chemistry community. The work is reported in a clear manner. I therefore recommend acceptance for this manuscript.

A couple of queries.
In the introduction you mention that the 4f electrons are shielded by the 5d shell. Is it not the 5s and 5p orbitals?

Response: Yes, the referee is right. 4f are shielded by 5s and 5p.

I feel it would be of exceptional interest if the authors could reveal the origin of the multiple relaxation processes that are observed. As the Dy(III) ions are crystallographically identical it is interesting that multiple processes are found. This analysis is however not trivial and an area of ongoing research. Have the Authors thought about looking into this further?

Response: We thank the referee for the suggestion and indeed the proper explanation for two step relaxation is not clear yet and also previous explanations of different crystallographic symmetry for multiple relaxation mechanism seems not adequate. So our compound (Dy2) can shed light on this topic. Yes, we have thought about this and we will make some DyY complex along with some theoretical calculations in order to check the cause of multiple relaxation process which is of course our future interest.

We hope that you will now find this revised version will be acceptable for publication in Dalton Trans.

Thanking you
Best regards
Chandrasekhar

Homodinuclear Lanthanide {Ln_2} (Ln = Gd, Tb, Dy, Eu) Complexes Prepared from a *o*-Vanillin based Ligand: Luminescence and Single-Molecule Magnetism Behavior

Prasenjit Bag,[a] *Chandresh Kumar Rastogi,*[b] *Sourav Biswas,*[a] *Sri Sivakumar,**[b,c] *Valeriu Mereacre**[d] *Vadapalli Chandrasekhar,**[a,e]

[a]Department of Chemistry, Indian Institute of Technology Kanpur, Kanpur-208016, India,

[b]Material Science Programme, Indian Institute of Technology Kanpur, Kanpur, India.

[c]Department of Chemical Engineering and Centre for Environmental Science and Engineering, Indian Institute of Technology Kanpur, Kanpur, India.

[d]Institute of Inorganic Chemistry, Karlsruhe Institute of Technology, Engesserstrasse 15, 76128 Karlsruhe, Germany.

[e]National Institute of Science Education and Research, Institute of Physics Campus, Sachivalaya Marg, Sainik School Road, Bhubaneshwar-751 005, Odisha, India

AUTHOR EMAIL ADDRESS: vc@iitk.ac.in; srisiva@iitk.ac.in

Abstract

Four dinuclear lanthanide complexes $[Gd_2 (H_2L)_2 (\mu\text{-piv})_2 (piv)_2]\cdot 2CHCl_3$ (**1**), $[Tb_2 (H_2L)_2 (\mu\text{-piv})_2 (piv)_2]\cdot 2CHCl_3$ (**2**), $[Dy_2 (H_2L)_2 (\mu\text{-piv})_2 (piv)_2]\cdot 2CHCl_3$ (**3**) and $[Eu_2 (H_2L)_2 (\mu\text{-piv})_2 (piv)_2]\cdot 2CHCl_3$ (**4**) were synthesized by the reaction of appropriate Ln(III) chloride salts and a multidentate ligand, 2,2'-(2-hydroxy-3-methoxy-5-methylbenzylazanediyl)diethanol (H_3L) in the presence of pivalic acid. **1-4** are neutral and are held by two monoanionic, $[H_2L]^-$ ligands. The two lanthanide ions are doubly bridged to each other via two phenolate oxygen atoms. Both the lanthanide ions are nine coordinated and possess a distorted capped square antiprism geometry. Photophysical studies reveal that Tb^{3+} (**2**) and Dy^{3+} (**3**) complexes display strong ligand-sensitized lanthanide-characteristic emission. The Tb^{3+} complex (**2**) shows a very high overall quantum yield of 76.2% with a life time of 1.752 ms. Magnetic studies reveal a single-molecule magnet behavior for **3** which shows in its ac susceptibility studies a two-step slow relaxation yielding two effective relaxation energy barriers of ΔE = 8.96 K and 35.51 K.

KEYWORDS: Amino-alcohol ligand; 4f complexes; Dinuclear complexes; Antenna-sensitized lanthanide emission; Antiferromagnetic coupling; Two-step slow relaxation of magnetization.

Introduction

There is a large interest in the development of lanthanide-based molecular materials for various applications such as large scale memory devices,[1] optoelectronic devices,[2] and biological systems[3] based on their unique luminescent and magnetic properties.[4] The magnetic properties of many lanthanide ion complexes arise from the large unquenched spin orbital angular momentum (of the lanthanide ions) and a consequent single-ion anisotropy along with a large ground-state spin.[5,4h] On the other hand, luminescence of lanthanide ion complexes arises from a variety of reasons including the effective shielding of the 4f shell electrons by the 5d, 5s and 5p orbitals, large excited-state lifetimes and large Stokes shifts.[6] Lanthanide ion-based single molecule magnets (SMMs) can be developed by manipulating the electronic structure of 4f-lanthanide ions by coordinating with organic ligands with multiple donating sites.[4h,7] SMMs containing Tb^{3+}, Dy^{3+}, Ho^{3+}, and Er^{3+} complexes are known. In particular, Dy^{3+}-based SMMs are common[8] compared to Tb^{3+} complexes[9] because Dy^{3+} is a Kramer ion in contrast to Tb^{3+} ion which is a non-Kramer ion.[4f,10] Ho^{3+} and Er^{3+}-based SMMs although known, are not very common.[11] In general, SMM properties and luminescence behaviour have been observed in different lanthanide complexes and only a few complexes are known where both the properties are exhibited.[14] This may be due to a lack of the antenna effect (energy transfer from ligand to Ln^{3+} ions)[12] which is an efficient process compared to direct excitation of Ln^{3+} ions due to their low extinction coefficients. It would be interesting to design lanthanide complexes that possess SMM behaviour along with good luminescent properties. Such complexes are likely to find applications in magneto-optical devices.[13] In a previous report, we have shown the utility of a flexible, *o*-vanillin-based ligand, H_3L to form heterometallic manganese-lanthanide complexes which showed SMM behavior.[15] It was apparent that this ligand would be effective for energy transfer to lanthanide ions such as Dy^{3+}. We were therefore interested if H_3L could be utilized to prepare homometallic lanthanide complexes with a view to discover both SMM and photoluminescence behaviour in the *same* complex. Accordingly, herein, the synthesis, structure and properties of $[Ln^{III}_2(H_2L)_2(\mu\text{-piv})_2(piv)_2]\cdot 2CHCl_3$ (Ln^{III} = Gd (**1**), Tb (**2**), Dy (**3**), Eu (**4**)) are reported. The Dy^{3+} derivative (**3**) shows the presence of a multi-step slow relaxation SMM behavior as well as a good

yellow luminescence (via antenna effect). Further, we find that the Tb^{3+} derivative (**2**) shows a very strong green luminescence (via antenna effect) with a quantum yield of ~76% and a lifetime of 1.75 ms. Both the complexes show very efficient energy transfer (~100%) in the sensitization process. The Eu^{3+}(**4**) and Gd^{3+}(**1**) complexes, on the other hand, do not show any lanthanide-characteristic emission properties.

Experimental Section

Reagents and general procedures

Solvents and other general reagents used in this work were purified according to standard procedures.[16] 2-Methoxy-4-methylphenol (Sigma Aldrich, USA) was used as purchased. Diethanolamine, and paraformaldehyde (S.D. Fine Chemicals, Mumbai, India) and $LnCl_3{\cdot}6H_2O$ (Aldrich Chemical Co. U.S.A. were used as such. 2,2'-(2-Hydroxy-3-methoxy-5-methyl-benzylazanediyl)diethanol (H_3L) was synthesized following a literature procedure.[15]

Synthesis

Preparation of the dinuclear complexes $[Ln^{III}_2(H_2L)_2(\mu\text{-piv})_2(piv)_2]$ (1−4)

A general protocol was implemented for the synthesis of the metal complexes (**1–4**) as follows: H_3L (0.102 g, 0.40 mmol) was dissolved in methanol (10 mL). $LnCl_3{\cdot}6H_2O$ (0.40 mmol) and triethylamine (0.18 mL, 0.12mmol) was added to this solution. The reaction mixture was stirred for 1 h. At this stage, pivalic acid (0.08 g, 0.8 mmol) was added, and the reaction mixture was stirred for a further period of 5 h at room temperature affording a white (**1-3**) and yellow (**4**) precipitate. This was filtered, washed with cold methanol (2 X 5 mL), dried and dissolved in 1:1 v/v mixture of chloroform and methanol. X-ray quality crystals of **1-4** were obtained within a week after slow evaporation of the solvent mixture. The characterization data for these complexes are given below.

$[Gd_2(H_2L)_2(\mu\text{-piv})_2(piv)_2]{\cdot}2CHCl_3$ (1)

Yield: 0.080 g (54.6 % based on Gd). Mp: >240 °C. IR (KBr), cm^{-1}: 3361 (b), 2957 (s), 2916 (m), 2864 (m), 1585 (s), 1539 (s), 1489 (s), 1419 (s), 1353 (s), 1333 (s), 1251 (s), 1226 (s), 1157 (s), 1099 (s), 1015 (s). ESI-MS *m*/*z*, ion: 1160.4, $[(LH_2)_2Gd_2piv_3 + MeOH]^+$. Anal. Calcd for $C_{48}H_{78}N_2O_{16}Cl_6Gd_2$ (1466.31 g mol^{-1}): C, 39.32; H, 5.36; N, 1.91%. Found: C, 39.02; H, 5.24; N, 1.84%.

$[Tb_2(H_2L)_2(\mu\text{-piv})_2(piv)_2]\cdot 2CHCl_3$ (2)

Yield: 0.084 g (57.1 % based on Tb). Mp: >240 °C. IR (KBr), cm^{-1}: 3333 (b), 2960 (s), 2917 (m), 2862 (m), 1586 (s), 1534 (s), 1489 (s), 1457 (m), 1418 (s), 1350 (s), 1333 (s), 1250 (s), 1226 (s), 1157 (s), 1100 (s), 1015 (s). ESI-MS *m*/*z*, ion: 1071.2, $[(LH_2)_2Dy_2piv_2+EtOH–3H]^-$1025.2, $[(LH_2)_2Tb_2piv_2–3H]^-$.Anal. Calcd for $C_{48}H_{78}N_2O_{16}Cl_6Tb_2$ (1469.68 g mol^{-1}): C, 39.23; H, 5.35; N, 1.91%. Found: C, 38.94; H, 5.24; N, 1.85%.

$[Dy_2(H_2L)_2(\mu\text{-piv})_2(piv)_2]\cdot 2CHCl_3$ (3)

Yield: 0.082 g (55.5 % based on Dy). Mp: >240 °C. IR (KBr), cm^{-1}:3319 (b), 2960 (s), 2917 (m), 2863 (m), 1587 (s), 1533 (s), 1490 (s), 1457(m), 1419 (s), 1350 (s), 1333 (s), 1250 (s), 1226 (s), 1158 (s), 1090 (s), 1016 (s). ESI-MS *m*/*z*, ion: 1079.2, $[(LH_2)_2Dy_2piv_2+EtOH–3H]^-$; 1033.2, $[(LH_2)_2Dy_2piv_2–3H]^-$.Anal. Calcd for $C_{48}H_{78}N_2O_{16}Cl_6Dy_2$ (1476.82 g mol^{-1}): C, 39.04; H, 5.32; N, 1.90%. Found: C, 38.69; H, 5.21; N, 1.82%.

$[Eu_2(H_2L)_2(\mu\text{-piv})_2(piv)_2]\cdot 2CHCl_3$ (4)

Yield: 0.076 g (52.2 % based on Ho). Mp: >240 °C. IR (KBr), cm^{-1}: 3374 (b), 2958 (s), 2918 (m), 2862 (m), 1584 (s), 1535 (s) 1489 (s), 1456 (w), 1419 (s), 1350 (s), 1333 (s), 1251 (s), 1225 (s), 1157 (s), 1099 (s), 1014 (s). ESI-MS *m*/*z*, ion: 1133.2, $[(LH_2)_2Eu_2piv_3 + H_2O]^+$.Anal. Calcd for $C_{48}H_{78}N_2O_{16}Cl_6Eu_2$ (1455.74 g mol^{-1}): C, 39.60; H, 5.40; N, 1.92%. Found: C, 39.21; H, 5.27; N, 1.84%.

Instrumentation

Melting points were measured using a JSGW melting point apparatus and are uncorrected. IR spectra (ESI, Fig. S20-23) were recorded as KBr pellets on a Bruker Vector 22 FT IR spectrophotometer operating at 400−4000 cm^{-1}. ^1H NMR was recorded on a JEOL-JNM LAMBDA model 400

spectrometer using $CDCl_3$ operating at 400 MHz. Elemental analyses of the compounds were obtained from Thermoquest CE instruments CHNS-O, EA/110 model. Electrospray ionization mass spectrometry (ESI-MS) spectra were recorded on a Micromass Quattro II triple quadrupole mass spectrometer. Electrospray ionization (both positive and negative ion, full scan mode) was used methanol, ethanol as solvent for desolvation. Capillary voltage was maintained at 2 kV, and cone voltage was kept at 31 kV.

Absorption and emission spectroscopic measurements were carried out at room temperature; the former using a Perkin-Elmer Lambda 45 UV-visible spectrophotometer and the latter using a SPEX Fluorolog HORIBA JOBIN VYON fluorescence spectrophotometer equipped with a double-grating 0.22 m Spex1680 monochromator and a 450 W Xe lamp as the excitation source. Photoluminescence life time measurements of **2** and **3** were carried out at room temperature using a SPEX Fluorolog HORIBA JOBIN VYON 1934 D phosphorimeter. Diffuse reflectance spectra were recorded on a UV-Vis VARIAN CARY 5000 spectrophotometer using $BaSO_4$ as a reference. Solid-state quantum yields were determined using the following equation:[17]

$$\Phi = (1-r_{st}/1-r_x)\,(A_x/A_{st})\,\Phi_{st} \qquad (1)$$

where r_x, r_{st} are reflectance values obtained from the diffuse reflectance spectra of the sample and the reference (with respect to a fixed wave length); Φ_{st} is the quantum yield of the reference; A_x and A_{st} are the integrated area under the emission spectra of complex and the reference. Quinine sulphate[18] was employed as the reference to determine the quantum yields of **2** and **3** in the solid-state.

X-ray Crystallography

The crystal data and the cell parameters for **1-4** are given in Table 1. The crystal data for **1-4** have been collected on a Bruker SMART CCD diffractometer using a Mo Kα sealed tube. The program *SMART*[19a] was used for collecting frames of data, indexing reflections, and determining lattice parameters, *SAINT*[19a] for integration of the intensity of reflections and scaling, *SADABS*[19b] for absorption correction, and *SHELXTL*[19c,d] for space group and structure determination and least-squares refinements on F^2. All the structures were solved by direct methods using the programs

SHELXS-97[19e] and refined by full-matrix least-squares methods against F^2 with *SHELXL-97*.[19e] Hydrogen atoms were fixed at calculated positions, and their positions were refined by a riding model. All the non-hydrogen atoms were refined with anisotropic displacement parameters. The crystallographic figures used in this manuscript have been generated using *Diamond 3.1e* software.[19f]

CCDC reference numbers for **1**–**4** are 1024774, 1024776, 1024775 and 1024777 respectively.

Magnetic Measurements

Magnetic susceptibility measurements were obtained with the use of a Quantum Design SQUID magnetometer MPMS-XL. This magnetometer works between 1.8 and 400 K for dc applied fields ranging from -7 to 7 T. Measurements were performed on polycrystalline samples. AC susceptibility measurements have been measured with an oscillating ac field of 3 Oe and ac frequencies ranging from 1 to 1500 Hz. The magnetic data were corrected for the sample holder.

Table 1. Details of the data collection and refinement parameters for compounds **1-4**.

	1	**2**	**3**	**4**
formula	$C_{48}H_{78}N_2O_{16}Cl_6Gd_2$	$C_{48}H_{78}N_2O_{16}Cl_6Tb_2$	$C_{48}H_{78}N_2O_{16}Cl_6Dy_2$	$C_{48}H_{78}N_2O_{16}Cl_6Eu_2$
M/g	1466.31	1469.68	1476.82	1455.74
crystal system	Monoclinic	Monoclinic	Monoclinic	Monoclinic
space group	$P2_1/c$	$P2_1/c$	$P2_1/c$	$P2_1/c$
Wavelength ($Mo_{K\alpha}$)	0.71069	0.71069	0.71069	0.71069
unit cell dimensions (Å , deg)	a = 10.800(5) b = 15.574(5) c = 18.284(5) α= 90.000(5) β= 95.473(5) γ = 90.000(5)	a = 10.789(5) b = 15.561(5) c = 18.269(5) α= 90.000(5) β= 95.279(5) γ = 90.000(5)	a = 10.758(5) b = 15.532(5) c = 18.285(5) α= 90.000(5) β= 95.275(5) γ = 90.000(5)	a = 10.842(2) b = 15.569(2) c = 18.273(2) α= 90 β= 95.541(2) γ = 90
V/Å^3	3061.3(19)	3054.1(19)	3042.4(19)	3070.0(7)
Z	2	2	2	2
ρ_c/g cm^{-3}	1.591	1.598	1.612	1.575

μ/mm^{-1}	2.471	2.621	2.763	2.347
F(000)	1476	1480	1484	1472
crystal size (mm^3)	0.15 x 0.125 x 0.105	0.128 x 0.107 x 0.089	0.148 x 0.12 x 0.092	0.15 x 0.13 x 0.105
θ range (deg)	4.08 to 25.02	2.64 to 25.50	2.24 to 26.00	1.89 to 25.50
limiting indices	-12<=h<=12, -11<=k<=18, -21<=l<=20	-13<=h<=12, -18<=k<=18, -22<=l<=15	-13<=h<=13, -19<=k<=18, -22<=l<=15	-11<=h<=13, -18<=k<=18, -22<=l<=16
reflns collected	15200	15921	16469	15898
Independent reflns	5339 [R(int) = 0.0338]	5611 [R(int) = 0.0369]	5905 [R(int) = 0.0414]	5665 [R(int) = 0.0476]
completeness to θ (%)	98.6	98.9	98.6	99.4
refinement method	Full-matrix least-squares on F^2	Full-matrix least-squares on F^2	Full-matrix least-squares on F^2	Full-matrix least-squares on F^2
data/ restraints/ params	5339 / 2 / 332	5611 / 0 / 350	5905 / 2 / 348	5663 / 4 / 318
goodness-of-fit on F^2	1.050	1.039	1.048	1.041
Final R indices [$I > 2\sigma(I)$]	R_1 = 0.0336, wR_2 = 0.0794	R_1 = 0.0332, wR_2 = 0.0782	R_1 = 0.0334, wR_2 = 0.0795	R_1 = 0.0415, wR_2 = 0.1022
R indices (all data)	R_1 = 0.0374, wR_2 = 0.0822	R_1 = 0.0403, wR_2 = 0.0828	R_1 = 0.0395, wR_2 = 0.0836	R_1 = 0.0512, wR_2 = 0.1102
largest diff. peak and hole(e ·Å^{-3})	1.484 and -1.001	1.761 and -0.798	1.919 and -0.816	1.524 and -1.091

Results and Discussion

Synthetic Aspects

The multisite coordinating ligand, H_3L, was synthesized by adapting a previous procedure reported by us[15] and involves the reaction of 2-methoxy-4-methylphenol, diethanolamine and paraformaldehyde. This ligand contains a phenol-frame work with two unsymmetrically disposed substituents. Adjacent to the phenol unit on one side is a diethanolamine group and on the other side, a methoxy group (Scheme 1). Thus, the ligand contains a total of five potential coordination sites: one nitrogen, one phenolate oxygen, two $-CH_2OH$ units and one methoxy oxygen. Among these, the weakly coordinating methoxy group has an inherent propensity to bind with the lanthanide ions specifically.

The flexible diethanolamine arms of the ligand containing three coordination sites, along with the phenolate oxygen atom, can effectively bind different metal centers with their versatile coordination action. Thus, while the *free* $N(CH_2CH_2OH)_2$ motif can bind as a terminal ligand, deprotonation can cause it to effectively bridge different metal centers. Previously it has been found that ethanolamine- or substituted diethanolamine-based ligands are quite useful for assembling both homometallic 3d and mixed metallic 3d/4f complexes.[20] Based on this, LH_3 was designed and used by us previously for the preparation of Mn_2Ln_2 complexes possessing an arch-type topology.[15] We were interested in preparing homometallic complexes with this ligand. Accordingly, we have found that H_3L reacts with $LnCl_3 \cdot 6H_2O$ in the presence of pivalic acid and triethylamine in a 1:1:2:4 stoichiometric ratio to afford neutral, homometallic dinuclear complexes $[(H_2L)_4Ln_2(piv)_4]$ (**1-4**) in excellent yields. ESI-MS of **1-4** was carried out to check if the structural integrity of the dinuclear core was maintained in solution. While the parent ion peaks could not be detected, we were able to find evidence for important fragments: $[(H_2L)_2Gd_2piv_3 + MeOH]^+$ (m/e:1160.4); $[(H_2L)_2Dy_2piv_2\text{-}3H]^-$ (m/e: 1033.2); $[(H_2L)_2Tb_2piv_2\text{-}3H]^-$ (m/e : 1025.2); $[(H_2L)_2Eu_2piv_3 + H_2O]^+$ (m/e:1133.2) (see Experimental Section; Supporting Information). The molecular structures of all the four complexes (**1-4**) were determined by single-crystal X-ray crystallography (vide infra). The presence of sharp peaks centered around 1585 and 1418 cm^{-1} in the IR spectra (ESI) can be assigned as arising due to the characteristic absorption of asymmetric ν_{as} (C=O) and ν_s (C=O) stretching vibration of bridging and terminal carboxylate groups .[21]

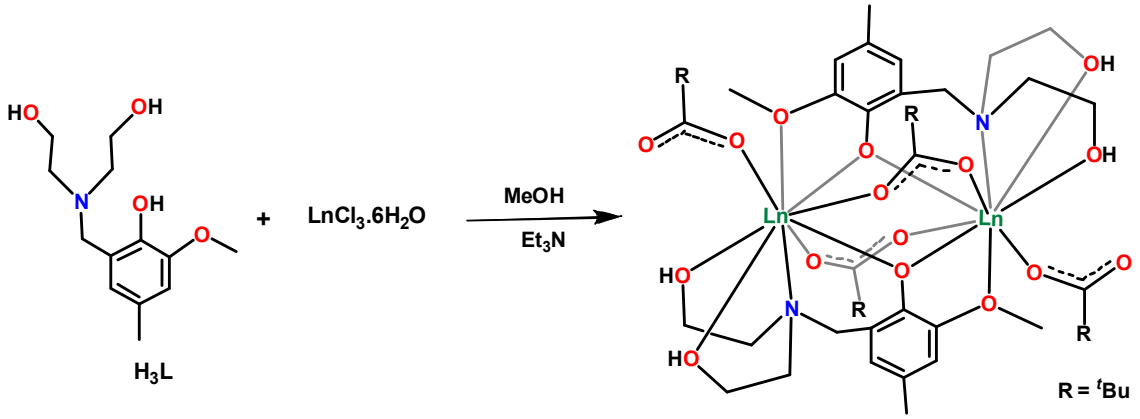

Ln = Gd(**1**), Tb(**2**), Dy(**3**), Eu(**4**)

Scheme 1. Synthesis of complexes **1-4**

Molecular Structures of 1-4

X-ray quality crystals of **1–4** were grown by a slow evaporation of the 1:1 (v/v) chloroform/methanol solution of the corresponding complexes. The X-ray data reveals that all of them crystallize in the monoclinic space group $P2_1/c$. The asymmetric unit of **1-4** consists of only half of the molecule viz., [Ln(H_2L)(μ-piv)(piv)] (Ln = Gd, Dy, Tb, Eu]. In view of the similarity of the molecular structures of **1–4**, we describe the structure of $[(H_2L)_2Gd_2(\mu\text{-piv})_2(piv)_2]\cdot 2CHCl_3$ (**1**) as a representative example. The structural features of this compound are detailed in Figs 1–3. Selected bond parameters of **1** are summarized in the caption of Figures 1 and 3. The molecular structures and significant bond parameters of the other compounds are given in the Supporting Information (Fig. S4-S6, Tables S2-S4).

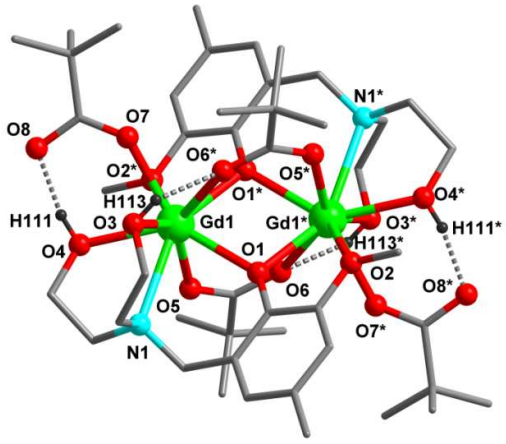

Fig. 1 Molecular structure of **1** (hydrogen atoms and solvent molecules are omitted for clarity).

Table 2. Intramolecular hydrogen bond parameters for compound **1**

	D-H….A	d(D-H) Å	d(H….A) Å	d(D….A)Å	<(DHA)°	Symmetry of A
1	O4-H111….O8	0.836(41)	1.727(46)	2.543(4)	164.89(38)	-x, 2-y, 1-z

	O3-H113….O6*	0.825(33)	1.914 (51)	2.534(4)	132.14(34)	-x, 2-y, 1-z

Two monoanionic ligands $[H_2L]^-$ are involved in holding the dimeric gadolinium unit together in **1** through two bridging phenolate oxygen atoms (Gd-O1 2.361(3) Å, Gd-O1* 2.333(3) Å; Gd-O-Gd* 102.71(10)˚ (Fig. 2). In addition, two pivalate ligands are also involved in holding the two centrosymmetrically related Gd^{3+} together (Gd(1)-O(5) = 2.386(3), Gd(1)-O(6)* = 2.486(3) Å). While one arm of the ligand (-OMe) binds to one Gd^{3+} (Gd(1)*-O(2) = 2.672(3) Å) the other arm containing the $[N(CH_2CH_2OH)_2]$ arm holds the other Gd^{3+} (Gd(1)-O(4) = 2.391(3), Gd(1)-O(3) = 2.546(3) Å). The two ethanolamine groups bind to Gd^{3+} in their free state. Finally, each Gd^{3+} has a unidentate pivalate ligand (Gd(1)-O(7) = 2.370(3) Å). Thus, each Gd^{3+} ion is nine coordinated (8O, 1N) in a distorted monocapped square-antiprism geometry. The O−Gd1−O angles vary from 71.79(9) to 143.72(9)°. The Gd-O bond distances, on the other hand, vary from 2.333(3) to 2.672(3) Å; the largest bond involves the –OMe group. The Gd(1)-N(1) bond distance 2.698(3) Å is longer than any of the Gd-O bonds.

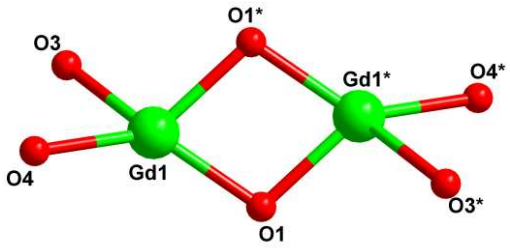

Fig. 2 View of the of the central Gd_2 core. Selected bond distances (Å) and bond angles (º): Gd(1)-O(4) = 2.391(3), Gd(1)-O(3) = 2.546(3), Gd(1)-O(1)* = 2.333(3), Gd(1)-O(1) = 2.361(3), Gd(1)-Gd(1)* = 3.665(2), Gd(1)*-O(1)-Gd(1) = 102.71(10), O(1)*-Gd(1)-O(3) = 132.62(9), O(1)-Gd(1)-O(4) = 138.59(9).

The crystal structure of **1** reveals the presence of intramolecular hydrogen bonds through the –OH group of the ethanolamine arm (O4-H111, O3-H113) with the oxygens (O8 and O6*) of both bridging and terminal carboxylate ligands. Further, a supramolecular polymeric 1D chain formed as a

result of intermolecular C-H…..O and C-H…..Cl interactions involving the solvent chloroform molecule (Supporting Information). All the hydrogen bond parameters are summarized in Table 2 and Supporting information (Table S4).

μ-η^1 : η^1 bridging bidentate **η^1** monodentate

Fig. 3 Different types of binding modes of pivalate anion towards Ln(III) ion.

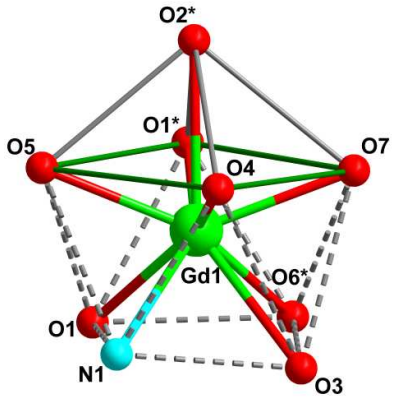

Fig. 4 Distorted capped-square-antiprism geometry around Gd1. Selected bond distances are as follows: Gd(1)-O(1)* = 2.333(3), Gd(1)-O(1) = 2.361(3), Gd(1)-O(7) = 2.370(3), Gd(1)-O(5) = 2.386(3), Gd(1)-O(4) = 2.391(3), Gd(1)-O(6)* = 2.486(3), Gd(1)-O(3) = 2.546(3), Gd(1)-O(2)* = 2.672(3), Gd(1)-N(1) = 2.698(3).

In this context it is interesting to mention that there are only four other phenoxo-bridged discrete Dy_2 complexes that are known in the literature which show interesting magnetic properties.[22] These are

given in Table 3. The metric parameters involved in the current instance are similar to those found in the literature and are summarized in Table 3.

Table 3. Some of the notable examples of the phenoxo-bridged dinuclear dysprosium complexes having SMM property.

Compound	$d_{Dy\cdots Dy}$(Å)	Dy-O_{bridge} bond length (Å)	Dy-O_{bridge}-Dy bond angle (˚)	Magnetic property U_{eff} (K), τ_0 (s)	ref
$[Dy(hfac)_3(\mu\text{-}pyNO)]_2$ [a]	4.071(2)	2.403	116.25	167, 5.62×10^{-11}	22a
$[Dy_2(ovph)_2Cl_2(MeOH)_3]$[a]	3.864 (5)	2.323-2.333	111.5-112.3	148.6, 2.3×10^{-8} 154.3, 7.3×10^{-9}	22b
$[Dy(valdien)(NO_3)]_2$ [a]	3.768(3)	2.31-2.33	108.22	76, 6.04×10^{-7}	22c
$[Dy_2(ovph)_2(NO_3)_2(H_2O)_2]$[a]	3.826(6)	2.319-2.348	110.2-113.15	69, 5.3×10^{-7}	22d
$[Dy_2(hmi)_2(NO_3)_2(MeOH)_2]$[a]	3.750 (4)	2.311-2.371	106.41	56, 3×10^{-7}	22e
$[Dy_2(H_2L)_2(\mu\text{-}piv)_2(piv)_2]$	3.633 (1)	2.337	103.02	8.96, 8.81×10^{-5} 35.51, 1.48×10^{-6}	This work

[a]Abbreviations: H_2ovph = ortho-vanillin picolinylhydrazone, H_2valdien = (*N1*,*N3*-bis(3-methoxysalicylidene)- diethylenetriamine), hfac = hexafluoro acetylacetone, hmi = 2-hydroxy-3-methoxyphenyl) methylene (isonicotino)hydrazine

Powder X-ray Diffraction (PXRD) and Thermogravimetric Analysis (TGA) Studies of 1-4.

In order to confirm the phase purity of the bulk samples in terms of their correspondance to the pure crystals of **1-3**, the powder X-ray diffraction analysis of these compounds were carried out (ESI, Fig. S24-26). The experimental PXRD spectra showed a reasonably good agreement with the simulated pattern (obtained from single-crystal data). Further, thermogravimetric analysis (TGA) were performed in order to check the thermal stability of all four (**1-4**) compounds. From the TGA data it is very evident that all the four compounds show similar type of stability/ decomposition pattern towards

heat treatment (ESI, Fig. S27). The TGA curves indicate two-step, gradual, weight loss process. The first step between 100 and 150 °C corresponds to a small weight loss, which is probably due to the loss of non-coordinated chloroform solvent molecules present in the crystal lattice. The second step, above 210-220 °C is indicative of a more rapid decomposition.

Photophysical Properties

UV-Vis spectra. The room temperature absorption spectra of all the four complexes (1×10^{-5} M) were recorded in dichloromethane solution revealing a strong absorption band with a red shift (peak maxima around 300 nm) due to $^{1}\pi$-π* transition compared to bare ligand (286 nm).[23] Furthermore, the molar absorption coefficients for all the complexes are found to be around 3.2×10^{4} M^{-1} cm^{-1} whereas the corresponding value for the ligand (H_3L) is 1.2×10^{4} M^{-1} cm^{-1}. This absorption band can be utilized to excite the lanthanide ions, this process can be more efficient than direct excitation.

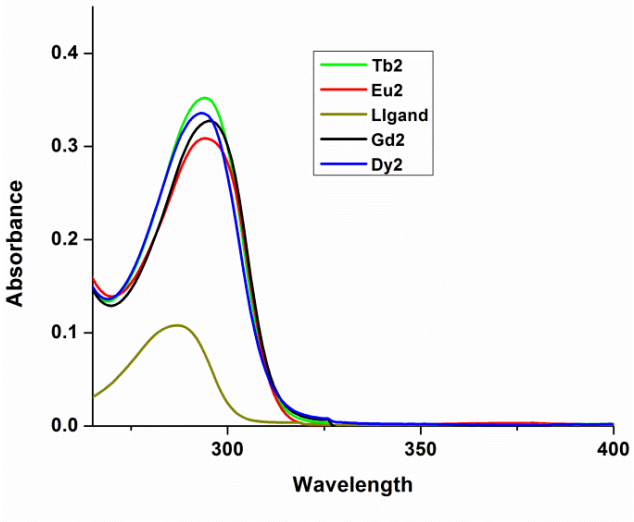

Fig. 5 UV-vis absorption spectra of all four compounds **1**(Gd_2), **2** (Tb_2), **3** (Dy_2) and **4** (Eu_2) including ligand (H_3L) (Concentration 1×10^{-5} M).

Lanthanide-centerd emission.

The excitation and emission spectra of the Dy^{3+} derivative (**3**) are shown in Figure 6a. The emission spectrum of the Dy^{3+} derivative (**3**) was recorded upon excitation with 300 nm UV light and shows characteristic emission of Dy^{3+}ions at ~ 482, 574, 660, and 750 nm due to $^4F_{9/2}\rightarrow{}^6H_J$ (J = 15/2, 13/2, 11/2, and 9/2) transitions respectively.[12b,24] The intense peak at ~574 nm is attributed to hypersensitive $^4F_{9/2}\rightarrow{}^6H_{13/2}$ transition which is strongly influenced by the local environment prevailing around Dy^{3+} ions.[14b, 24c] The luminescence decay curve was recorded by monitoring emission at 574 nm for the life time estimation and is shown in Figure 6b. The obtained curve was well fitted with a single exponential function to provide a life time value of τ_{obs} = 11.0 μs which is one of the higher values reported in the literature.[14, 24] The single exponential fit provides evidence of a single type of Dy^{3+} emitting centre in **3**. The overall quantum yield for this sensitized emission was estimated by equation 1 and is found to be to be 2.74 % (Table 4). The excitation spectrum recorded by monitoring the emission at 574 nm ($^4F_{9/2}\rightarrow{}^6H_{13/2}$) shows a strong band ranging ~ 320-270 nm with peak at ~ 300 nm with a very weak excitation peaks of Dy^{3+} ions. The strong absorption band at ~ 300 nm is attributed to the π-π* transition of the ligand which is much more efficient than the direct *f-f* absorption of Dy^{3+} ions. The presence of typical strong ligand-characteristic absorption band signifies efficient energy transfer from the ligand to the metal centre in compound **3**.

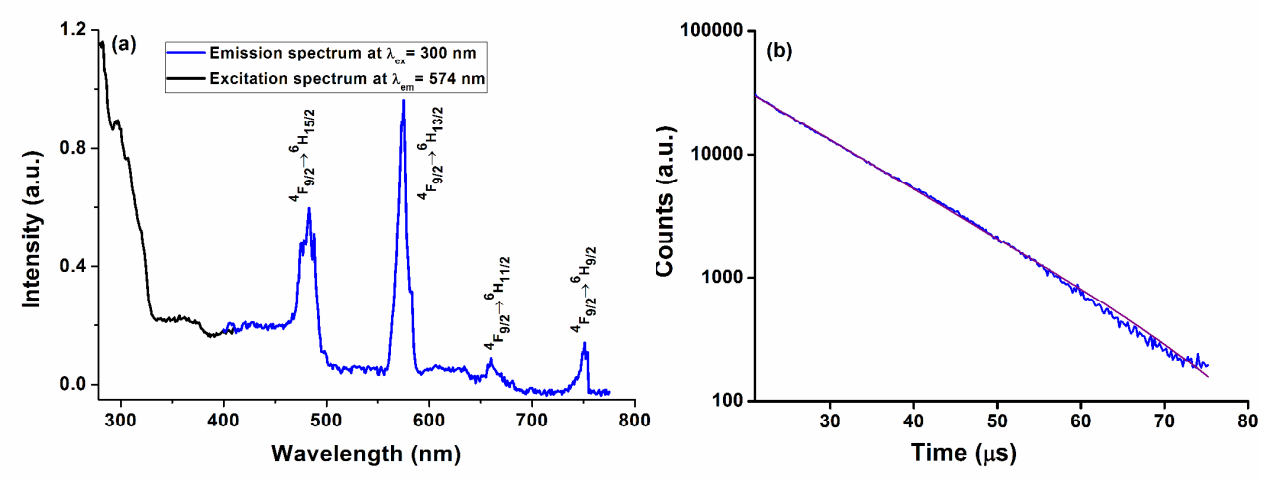

Fig. 6 (a) Room temperature excitation spectrum (λ_{em} = 574 nm) and emission spectrum (λ_{ex} = 300 nm) and (b) phosphorescence decay profile (blue curve) (λ_{em} 574 nm and λ_{ex}= 300 nm) of the Dy^{3+}compound (**3**). The solid red line represents mono-exponential fit to the decay curve.

The room temperature emission spectrum of Tb^{3+} derivative (**2)** was recorded upon excitation with 300 nm UV light and is shown in Fig. 7a. This spectrum shows a strong Tb^{3+} characteristic emission in the visible region having peaks at ~ 488, 545, 586, 620, 650, 667 and 680 nm attributed to $^5D_4 \rightarrow {}^7F_J$ (J = 6-0) transitions of the Tb^{3+} ions.[12b,25] The most intense peak at 545 nm is due to the $^5D_4 \rightarrow {}^7F_5$ transition. The weak peak at 488 nm is due to the electric dipole transition $^5D_4 \rightarrow {}^7F_6$ and is also highly sensitive to the chemical environment and symmetry of the coordination polyhedron around the terbium ion.[24c] Moreover, no residual emission was detected from the ligand part, suggesting a complete ligand to metal energy transfer process in the compound **2**. The luminescence lifetime (τ_{obs}) of the excited state of Tb^{3+} ions ($^5D_4$) was estimated by recording the decay curve (shown in Fig. 7b) by monitoring the 545 nm emission ($^5D_4 \rightarrow {}^7F_5$ transition) of Tb^{3+} ions. The decay profile was well fitted with the single exponential function revealing one type of emitting centre in the Tb^{3+} derivative (**2)** and the estimated lifetime was found to be 1.75 ms which is quite high in comparison to those reported in literature for other Tb^{3+} complexes. The overall quantum yield for this sensitized emission was estimated by equation 1 and is found to be high (~76.18 %). The excitation spectrum of Tb^{3+} derivative (**2)** was recorded by monitoring the emission at 545 nm ($^5D_4 \rightarrow {}^7F_5$) which shows a broad excitation band in the range 320-270 nm having peak around 300 nm (Figure 7a). The absorption band at ~ 300 nm is attributed to the π-π^* transition of the ligand and is strong enough such that the other excitation peaks corresponding to the absorption of Tb^{3+} ions are not clearly visible in this case. The presence of typical ligand-characteristic absorption band signifies efficient energy transfer from ligand to metal in compound **2.** We note that Eu^{3+} and Gd^{3+} complexes did not show any emission which may be due to Latva's rule (see below for detailed explanation).[26]

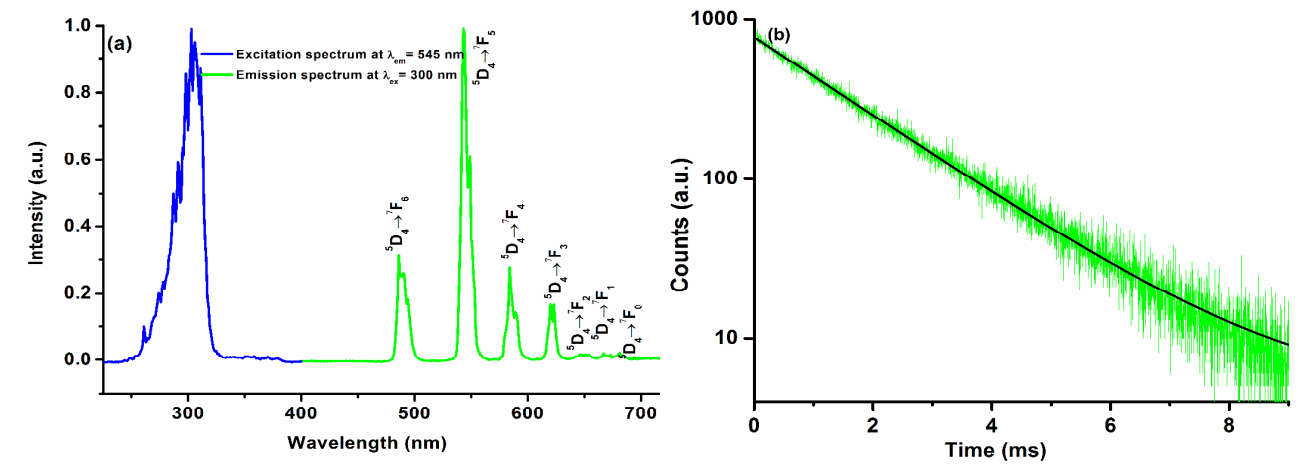

Fig. 7 (a) Room temperature excitation spectrum (λ_{em} = 545 nm) and emission spectrum (λ_{ex} = 300 nm) and (b) phosphorescence decay profile (blue curve) of Tb^{3+} derivative, **2** (λ_{em}= 545 nm and λ_{ex}= 300 nm). The solid black line represents mono exponential fit to the decay curve.

Additionally, the sensitization efficiency (η) of the ligand chromophore for the Tb^{3+} and Dy^{3+} complexes has been estimated using the following equation[27]

$$\eta = 1 - \tau_a/\tau_0 \qquad (2)$$

Where τ_a and τ_0 are the luminescence lifetimes of the donor (corresponding to 410 nm emission of H_3L) in the presence and absence of the acceptor respectively.

In order to find out the τ_0 value we have chosen the Gd^{3+} complex because there is no energy transfer from the ligand to Gd^{3+} ion and the complex possesses a structure similar to the Dy^{3+}/Tb^{3+} complexes. The estimated lifetime of the excited state of ligand in absence (τ_0) and in presence of Dy^{3+} and Tb^{3+} ions (τ_a) was found to be 250 μs, 1.56 μs and 1.38 μs respectively. The sensitization efficiency of ligand (H_3L) in the compounds Tb^{3+} (**2**) and Dy^{3+} (**3**) were estimated using Equation 2 and is found to be 99.3 and 99.4 % respectively (Table 4). The above data suggests efficient energy transfer from the ligand chromophore to Tb^{3+} and Dy^{3+} ions in complexes **2** and **3** respectively.

Table 4. Estimated luminescence lifetime, sensitization efficiency and overall quantum yield data for Tb^{3+} and Dy^{3+} derivatives (complexes **2** and **3** respectively).

S.No.	Complex	Absorbance λ [nm] ($10^{-4}\times \varepsilon_{max}$) in solution	Life time (τ) (μs) λ_{ex} = 300 (nm)	Sensitization efficiency of the ligand (η_{sen})	Overall quantum yield (φ)
1	**2**	298 (3.518)	1752 (λ_{em} = 545 nm)	0.993	0.762
2	**3**	296 (3.374)	11 (λ_{em} = 574 nm)	0.994	0.027

Mechanism for sensitized emission

In the sensitization mechanism, for an effective energy transfer to occur from the triplet state of the ligand chromophore to the emitting level of lanthanide ion four steps are involved:[28] i) excitation of the organic chromophore to its higher excited state ($S_0 \rightarrow S_1$) using UV/high-energy visible light, ii) intersystem crossing in the ligand excited state to its triplet state ($S_1 \rightarrow T_1$) iii) triplet state energy transfer to the resonant levels of Ln(III) ion via a non-radiative pathway, iv) radiative emission from the lanthanide ions. The third and final step is the most crucial to determine the luminescence efficiency of lanthanide ions.[29] Other than the above four criteria another factor is the presence of vibrational oscillators such as –OH and –NH in the coordination sphere of the lanthanide ion, which are quite effective in quenching the luminescence and excited state life time of lanthanide ions.[12b,30] Therefore, Ln(III) complexes, to be utilized in photophysical applications, must not contain coordinating water molecules/other molecules that possessing vibrational oscillators. Crystallographic data of complexes **1-4**, suggest the absence of water molecules and other vibrational oscillators in direct coordination sphere of the lanthanide ions. However, presence of terminal OH coordinating groups emanating from the diethanolamine arm can quench the luminescence. From the emission studies of **2-4** (Fig. 6a, 7a and ESI, Fig. S10) it is evident that the antenna effect occurs for compounds **2** and **3** producing green and yellow emission respectively. On the other hand, Gd^{3+} and Eu^{3+} complexes did not show their characteristic emission. In order to assess the overall energy

transfer process we need to know the singlet and triplet energy levels of the ligand chromophore. The first excited singlet energy level ($^1\pi\pi^*$) and the triplet energy ($^3\pi\pi^*$) level of the ligand was determined as 320 nm (31250 cm^{-1}) and 390 nm (25640 cm^{-1}) respectively from the UV-Vis absorption spectrum (Fig. 5) and low temperature luminescence spectra (78 K) of Gd^{3+} complex (Fig. 8). This gives a singlet-triplet ($^1\pi\pi^*$-$^3\pi\pi^*$) energy gap around 5610 cm^{-1}. Therefore this is in accordance with the Reinhoudt's empirical rule ($^1\pi\pi^*$-$^3\pi\pi^*$ > 5000 cm^{-1}) for effective inter system crossing (ISC).[31] Also the triplet energy level of the ligand is well above the emitting level of Tb^{3+} ($^5D_4$: 20400 cm^{-1}) and Dy^{3+} ($^4F_{9/2}$: 20800 cm^{-1}), giving a possibility for effective energy transfer for the two compounds, **2** and **3**. The assignment of overall energy transfer process can be further corroborated from the excitation spectra of compounds **2** and **3** (Fig. 7a and 6a). Upon direct excitation at the *f-f* sublevels (at the characteristics emission maxima) of Tb^{3+} and Dy^{3+} only the ligand- characteristic absorption bands (around λ = 300 nm) originating from the $^1\pi\pi^*$ transition, are seen (Fig. 5). It is well known that the lowest-lying excited energy level ($^6P_{7/2}$) for Gd^{3+} is located at 32150 cm^{-1} which is higher than the singlet energy level, prohibiting any antenna effect for this complex.[32] So the luminescence we get is basically ligand-based phosphorescence which is further confirmed from life time (τ) measurements which is similar to the ligand (τ = 1.29 ms) at lower temperature.

On the other hand, absence of luminescence from Eu^{3+} may be attributed to the transient formation of Eu^{2+} from Eu^{3+} ion due to ligand to metal charge transfer (LMCT) from the phenolate to Eu^{3+} ion.[33] This is further confirmed by the presence of a weak broad emission band at ~ 450 nm which may be attributed to Eu^{2+} ion. In addition, the life time of this emission (1.38 μs) is much lower than the lifetime of ligand (250 μs). This is further confirmed by the absence of Eu^{3+} emission by exciting the Eu^{3+} ions directly at *f-f* energy level of Eu^{3+} at 395 and 464 nm (ESI, Fig. S11). The whole energy transfer pathway is depicted in Fig. 9.

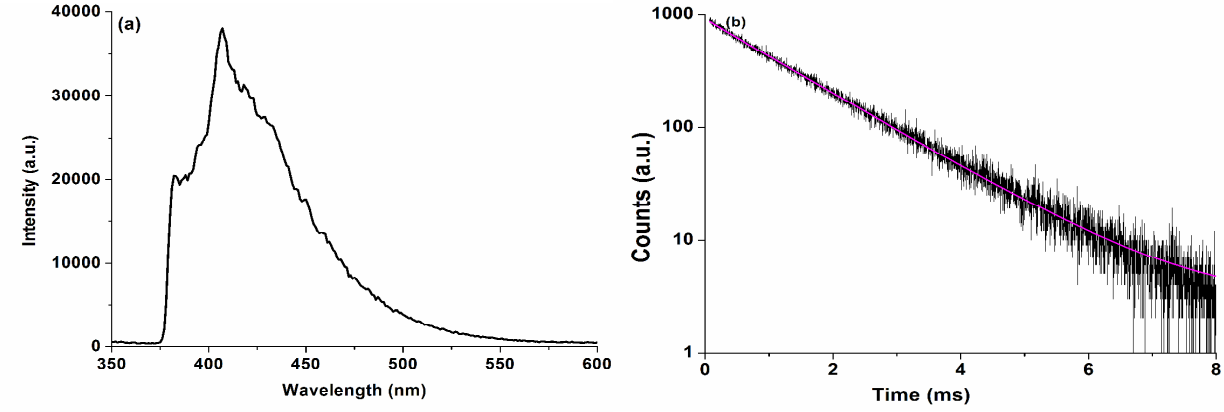

Fig. 8 Low temperature (78 K) (a) phosphorescence spectra and life time decay profile of (b) Gd_2 (**1**) compound (λ_{ex}= 300 nm). The emission was monitored at 410 nm (The solid violet line represent monoexponential fit to the decay curve.

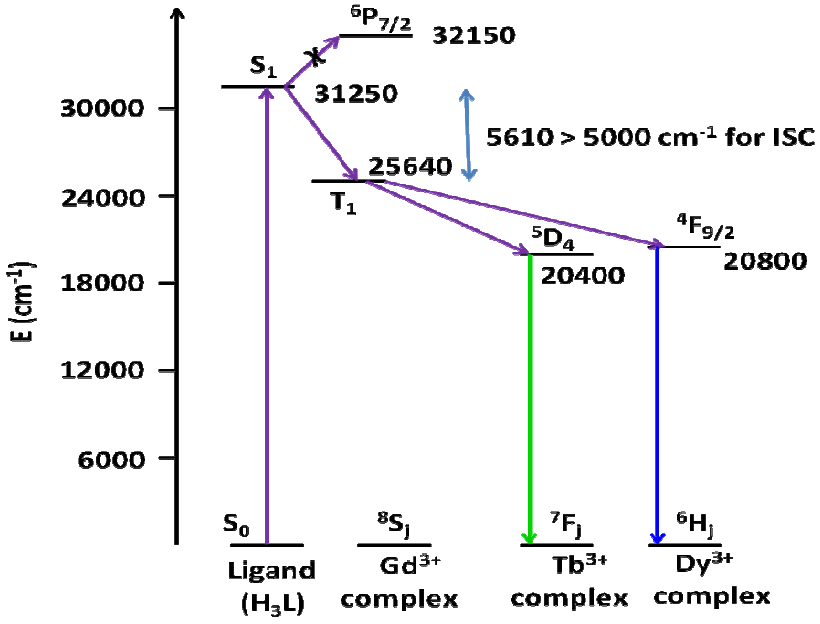

Fig. 9 Schematic representation of the overall energy transfer process in complexes **1-3**.

Magnetic Properties

The dc magnetic susceptibility properties of Gd^{3+}, Tb^{3+} and Dy^{3+} complexes (**1-3)** were investigated in the temperature range 1.8-300 K with an applied magnetic field of 1000 Oe, and the results are displayed in Fig. 10. Field dependence of the magnetization for all the complexes between 2 and 5 K are shown in Figures S1-S3, Supporting Information. At room temperature, the χT values of complexes **1-3** are 15.8, 24.6, and 29.2 $cm^3K\ mol^{-1}$, respectively. These values are in good agreement with the theoretical values (**1**: 15.76; **2**: 23.64; **3**: 28.34 $cm^3\ K\ mol^{-1}$) for two non-interacting lanthanide ions: Gd(III) ($^8S_{7/2}$, $S = 7/2$, $L = 0$, $g = 2$, $C = 7.88\ cm^3\ K\ mol^{-1}$), Tb(III) ($^7F_6$, $S = 3$, $L = 3$, $g = 3/2$, $C = 11.82\ cm^3\ K\ mol^{-1}$) and Dy(III) ($^6H_{15/2}$, $S = 5/2$, $L = 5$, $g = 4/3$, $C = 14.17\ cm^3\ K\ mol^{-1}$).[34]

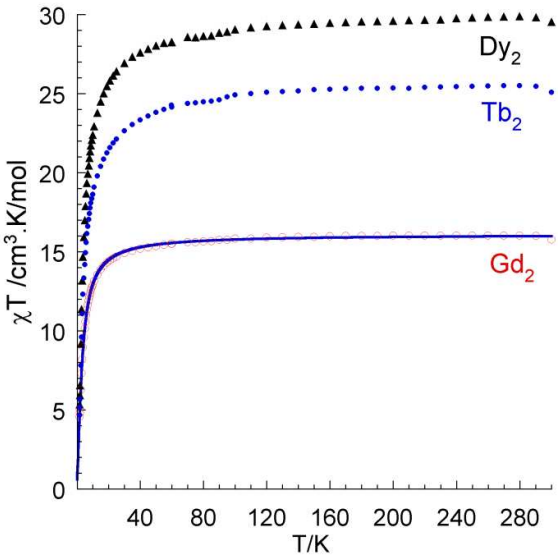

Fig. 10 Temperature dependence of the χT product at 1000 Oe for complexes **1** (Gd_2), **2** (Tb_2), **3** (Dy_2). Solid blue line represents the best fit of the experimental susceptibility data for compound **1**with $J_{GdGd} = -0.19\ (1)\ cm^{-1}$ and $g = 2.0\ (2)$ (see text).

For all the compounds, on lowering the temperature, χT values stay almost constant with decreasing temperature down to approximately 50-60 K, below which it decreases considerably, reaching a value of ~ 5.0 $cm^3\ K\ mol^{-1}$ at 1.8 K. For the Gd^{3+} compound (**1),** such a behaviour can be attributed to the weak antiferromagnetic exchange coupling between the Gd^{III} ions or zero-field splitting effects.[35]

Here the two Gd(III) ions are tetra bridged via two pivalate and two phenolate ligands. Therefore, the exchange pathway between the Gd(III) ions is occurring mainly through the O-bridge.

In order to understand the magnetic exchange interaction in Gd_2 (**1**) unit we simulated the temperature dependence of the magnetic susceptibility of **1**. Taking into account the structural parameters of **1** the general spin-Hamiltonian describing the isotropic exchange interactions can be written as:

$$H = -J\,\mathbf{S}_{Gd1}\cdot\mathbf{S}_{Gd2} \qquad (3)$$

J is the intramolecular magnetic exchange interaction involving Gd….Gd centres. The D_{Gd} (anisotropy) is assumed to be negligible as the Gd^{3+} ion is rather isotropic because of the lack of any first-order orbital momentum for the Gd(III) ions. The best fit of the experimental susceptibility data (Fig. 10) with the above Hamiltonian yielded the parameters: J = -0.19(1) cm^{-1}, g = 2.0(2) with a very good agreement factor R =2.4x10^{-3}. The results of J and g values are comparable with those earlier reported for polynuclear phenoxo and pivalate bridged Gd^{III} complexes[36] ; the low exchange coupling constants are because of the limited radial extension of their inner f orbitals. Further, the magnetization measurements at low temperatures reveal a saturation of 6.8 μ_B at 7 T, a value close to the expected saturation value of M_s = 7.0 μ_B (g = 2.00) (Fig. S16). This further confirms the occurrence of very weak antiferromagnetic interactions taking place in the Gd_2 compound. Because of the very weak exchange interaction (J = - 0.19(1) cm^{-1}) the saturation value can be obtained at very low temperatures.

On lowering the temperature, χT values for compounds **2** and **3**, remain almost constant up to 100 K then continuously decreases when the temperature is reduced with a more rapid fall below 40 K, reaching 4.5 $cm^3\,mol^{-1}$ K and 5.0 $cm^3\,mol^{-1}$ K at 2 K respectively (Figure 10). This behaviour is typical for Ln(III) ions with an unquenched orbital moment and can originate from several contributions like thermal depopulation of the excited m_J sublevels of the $^{2S+1}\Gamma_J$ ground state of the Ln^{3+} ion originated by crystal field symmetry i.e. site symmetry around Ln(III) ion, in conjunction with the weak $Ln^{3+}\cdots Ln^{3+}$ antiferromagnetic interactions in **2** and **3**. The presence of weak

antiferromagnetic interaction in these two compounds cannot be excluded in view of the fact that they are isostructural with the gadolinium derivative (**1**).[37]

The linear variation and non-saturation of the field dependent magnetization for compounds **2** and **3** at 2 K (ESI, Fig. S16, S17) shows a rapid increase of the magnetization at low field and a linear increase at high field to reach values of the magnetization at 7 T to 10.5 and 11.5 $N\mu_B$ for compounds **2** and **3**, respectively. These values are considerably smaller than the expected saturation magnetization values, $Ms/N\mu_B = 2g_J J$, for two Ln^{3+} ions. The large discrepancy from the expected magnetization saturation values points out to the presence of significant magnetic anisotropy and/or more likely presence of low lying excited states that are partially (thermally and field-induced) populated.[38]

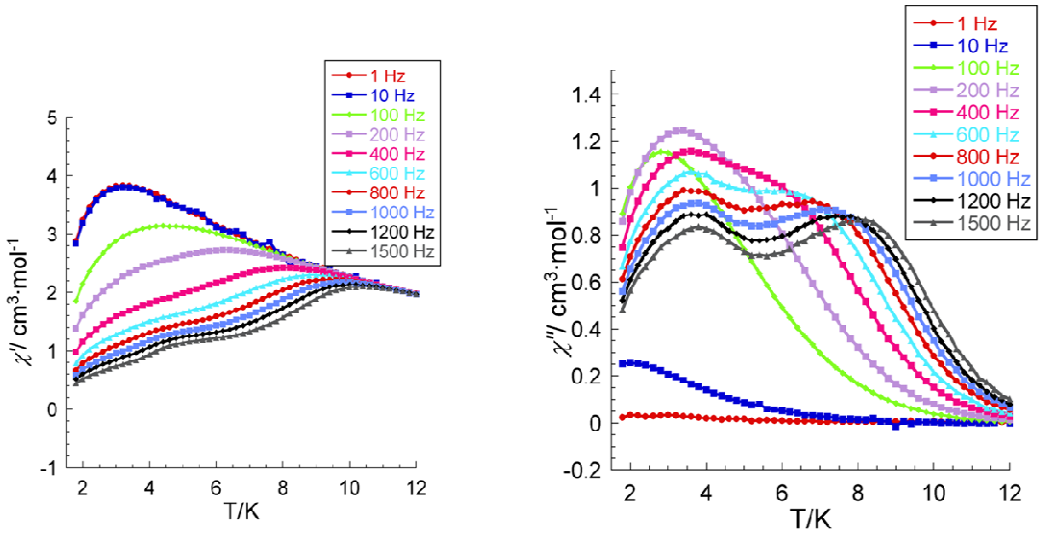

Fig. 11 Temperature dependence of the out-of-phase ac signals (χ''_M) under zero applied dc field for **3**. Solid lines are a guide to the eye.

To explore the presence of slow relaxation of the magnetization, dynamic ac magnetic susceptibility measurements as a function of temperature at variable frequencies were performed on microcrystalline powder samples of all the three complexes (**1-3**) in the temperature range 1.8-12 K with zero dc field and a 3 Oe ac field at 1-1500 Hz. But among them only compound **3** shows slow relaxation of the magnetization as it is evident from the AC susceptibility data (Fig. 11). On the other

hand compound **2** did not show either frequency or temperature dependent out-of-phase ac signal revealing its non SMM nature. This clearly indicates that the energy barrier for flipping of magnetization for compound **2** is not enough to trap the magnetization in one side of the potential well in order to show SMM behaviour i.e. flipping rate is too high to observe the signal in the χ_M'' plot above 2 k. However, the ac data of compound **3** showed occurrence of two peaks with maxima for χ_M'' centered at 3.8 and 8.0 K for 1500 Hz, showing that two relaxation processes take place in this compound. Such a behavior can be ascribed to the presence of two Ln sites. But the structure reveals that two Dy sites are surrounded by the same ligand field environment, i.e. both Dy^{3+} ions are crystallographically equivalent and therefore only one relaxation process is expected. Nevertheless the presence of two relaxation process with a single chemical environment around Ln^{3+} ion is well documented in some instances.[39]

The effective energy barrier (U_{eff}) for magnetization reversal and the time constant (τ_0) both at high (HT) and low temperature (LT) have been evaluated from the plot of $\chi'' = f(\nu)$ curve as $\ln(\tau) = f(T^{-1})$, are aligned where $\tau = 1/2\pi\nu$ is the corresponding relaxation time for a given frequency ν. By fitting these two curves (Figure 12) to the Arrhenius expression $\tau = \tau_0 \exp(U_{eff}/kT)$, we are able to extract two energy barriers, U_{eff} = 8.96 K and 35.5 K with two pre-exponential factor $\tau_0 = 8.81\times10^{-5}$ s and 1.48×10^{-6} s at low and high temperature respectively. Arrhenius analysis confirms that both processes are thermally activated, but the τ_0 value obtained for the LT is bigger than expected for a SMM[14c,40] and suggests that this process is dominated by the quantum pathway of relaxation.

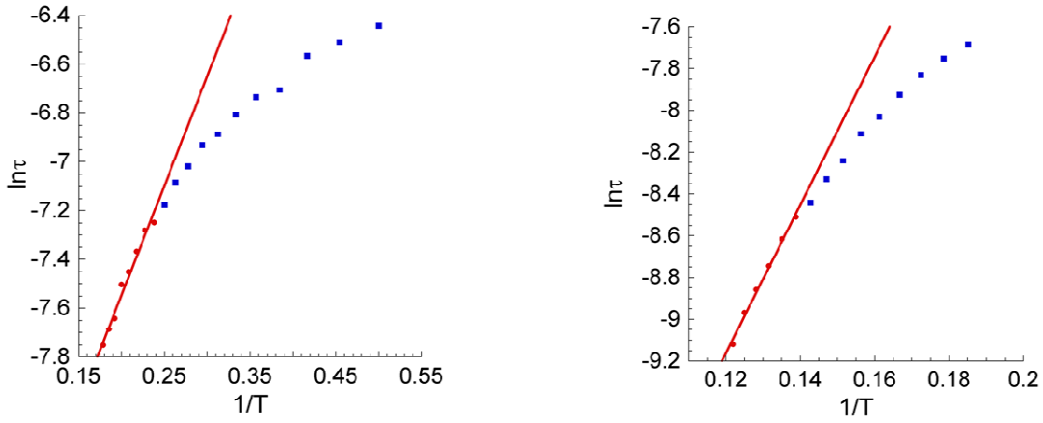

(a) (b)

Fig. 12 Plots of inverse temperature vs the natural log of the two relaxation time:(a) low temperature, (b) high temperature region of compound **3**. Red lines represent fits to the Arrhenius expression $\ln(\tau) = \ln(\tau_0) + U_{eff}/k_BT$.

The relatively low energy barriers for magnetization reversal of compound **3**, compared to the other phenoxo- bridged dinuclear lanthanide complexes (Table 3) can be attributed to the low symmetry of the ligand field around the Dy^{3+} ion resulting in low single ion anisotropy ultimately responsible for fast relaxation and hence the low energy barrier.

The low and high temperature frequency-dependent ac susceptibility data (ESI, Fig. S16) for compound **3** was further analyzed using a generalized Debye model to fit the Cole-Cole plot (Supporting Information, Fig. S19).[41] The Cole–Cole plot, between 2 - 5.2 K, shows an almost semicircle corresponding to the FR (fast relaxation) whereas in the temperature range between 5.6-8.8 K the plot deviates from a semicircle. The best fit of the Cole-Cole plot using the generalized Debye model in the two temperature regions afforded the α values in the ranges of 0.15 (2K) –0.07 (5.2 K) and 0.05 (5.6 K) – 0.03 (8.8 K). The former α values supports much broader distribution i.e. multiple relaxation processes at low temperature because both quantum tunnelling and Orbach processes are operating. On the other hand at higher temperature relatively narrow distribution of the relaxation times have been found.

Finally, from the ac data it is very evident that while **3** shows an interesting two-step relaxation SMM behavior, **2** does not show any temperature-dependent out-of-phase ac signal revealing its non SMM behavior although both Dy^{3+} and Tb^{3+} ions are highly anisotropic in nature. This difference in magnetic behavior is presumably due to the fact that Dy(III) is a Kramer ion and irrespective of the ligand field symmetry it is expected to possess a bistable ground state, whereas, Tb(III) ion is a non-Kramer ion. So its complex will possess a bistable ground state only if it is present in a highly axial symmetry ligand field.[4f,10]

Conclusion

In summary, we have synthesized four homodinuclear neutral lanthanide complexes $\{Ln_2\}$ using a multidentate ligand, 2,2'-(2-hydroxy-3-methoxy-5-methylbenzylazanediyl)diethanol (LH_3) that was built on a *o*-vanillin platform. All the four compounds (**1-4**) are centrosymmetric in nature and are held by two monoanionic ligands $\{LH_2\}^-$ in conjunction with four pivalate anions. The overall coordination action of the two dianionic ligands and the pivalate anion produces a distorted capped square-antiprism geometry (8O, 1N) around each Ln^{3+} ion. Detailed photophysical measurements showed that only compounds **2** and **3** are sensitized by the ligand chromophore and therefore show their strong lanthanide characteristic emission. The Eu^{3+} ion remains unsensitized in compound **4** and this is probably due to the transient formation of Eu^{2+} from Eu^{3+} ion due to ligand to metal charge transfer (LMCT) from the phenolate to Eu^{3+} ion. Magnetic studies revealed that compound **3** shows a SMM behavior with two step relaxations process, the high temperature one being thermally activated and the low temperature one being dominated by the quantum pathway of relaxation. In comparison to compound **3**, compounds **1** and **2** do not show slow relaxation of the magnetization.

Acknowledgements

V.C. is thankful to the Department of Science and Technology, for a J. C. Bose fellowship. P. B. and S.B. thank Council of Scientific and Industrial Research, India for a Senior Research Fellowship.

References

1 (a) A. Candini, S. Klyatskaya, M. Ruben, W. Wernsdorfer, M. Affronte, *Nano Lett*., 2011, **11**, 2634; (b) J. Tejada, E. M. Chudnovsky, E. del Barco, J. M. Hernandez, T. P. Spiller, *Nanotechnology*, 2001, **12**, 181; (c) M. Mannini, F. Pineider, P. Sainctavit, C. Danieli, E. Otero, C. Sciancalepore, A. M. Talarico, M.-A. Arrio, A. Cornia, D. Gatteschi, R. Sessoli, *Nature Mater*., 2009, **8**, 194.

2 (a) L. D. Carlos, R. A. S. Ferreira, V. de Zea Bermudez, B. Julian-Lopez, P. Escribano, *Chem. Soc. Rev.*, 2011, **40**, 536; (b) D. A. Cristaldi, S. Millesi, P. Mineo, A. Gulino, *J. Phys. Chem. C*, 2013, **117**, 16213; (c) H. Wei, G. Yu, Z. Zhao, Z. Liu, Z. Bian, C. Huang, *Dalton Trans.*, 2013, **42**, 8951; (d) L. Wu, Y. Zhang, M. Gui, P. Lu, L. Zhao, S. Tian, Y. Kong, J. Xu, *J. Mater. Chem.*, 2012, **22**, 6463; (e) A. de Bettencourt-Dias, *Dalton Trans.*, 2007, 2229.

3 (a) G. Mathis, *Rare earths, in:* R. Saez-Puche, P. Caro, (Ed.), Editorial Complutense, Madrid, Spain, 1998; (b) S. Aime, S.G. Crich, E. Gianolio, G. B. Giovenzana, L. Tei, E. Terreno, *Coord. Chem. Rev*. 2006, **250**, 1562; (c) V. W. W. Yam, K. K.W. Lo, *Coord. Chem. Rev*., 1999, **184**, 157; (d) S. V. Eliseevaa, J. -C. G. Bünzli, *Chem. Soc. Rev*., 2010, **39**, 189; (e) J. -C. G. Bünzli, *Chem. Rev.*, 2010, **110**, 2729.

4 (a) J.C.G. Bunzli, C. Piguet, *Chem. Soc. Rev.*, 2005, **34**, 1048; (b) M. D. Ward, *Coord. Chem. Rev*., 2007, **251**, 1663; (c) M. Sakamoto, K. Manseki, H. Okawa, *Coord. Chem. Re*v., 2001, **219**, 379; (d) R. Sessoli, A. K. Powell, *Coord. Chem. Rev*. 2009, **253**, 2328; (e) C. Benelli, D. Gatteschi, *Chem. Rev*., 2002, **102**, 2369; (f) D. N. Woodruff, R. E. P. Winpenny, R. A. Layfield, *Chem. Rev.*, 2013, **113**, 5110; (g) R. Winpenny, *Single-molecule Magnets and related Phenomena*; Springer-Verlag Berlin Heidelberg: Germany,**2006**; (h) J. D. Rinehart, J. R. Long, *Chem. Sci*. 2011, **2**, 2078.

5 (a) M. Murugesu, *Nat. Chem*., 2012, **4**, 347; (b) M. Nakano, H. Oshio, *Chem. Soc. Rev*., 2011, **40**, 3239.

6 (a) X.-P. Yang, R. A. Jones, *J. Am. Chem. Soc.*, 2005, **127**, 7686; (b) J.-C. G. Bünzli, *in Lanthanide Probes in Life, Chemical and Earth Science, eds*. J.-C. G. Bünzli, G. R. Choppin, Elsevier Science Publ. B.V., Amsterdam, 1989, ch. 7; (c) N. Sabbatini, M. Guardigi, F. Bolletta, I. Manet, R. Ziessel, *Angew. Chem., Int. Ed.*, 1994, **33**, 1501; (d) S. Cotton, *Lanthanide and Actinide Chemistry*; John Wiley & Sons: West Sussex, U. K., 2006.

7 J. J. Baldoví, S. C. Serra, J. M. Clemente-Juan, E. Coronado, A. Gaita-Ariño, A. Palii, *Inorg. Chem*., 2012, **51**, 12565.

8 (a) R. J. Blagg, C. A. Muryn, E. J. L. McInnes, F. Tuna, R. E. P. Winpenny, *Angew. Chem., Int. Ed*., 2011, **50**, 6530; (b) R. J. Blagg, L. Ungur, F. Tuna, J. Speak, P. Comar, D. Collison, W. Wernsdorfer, E. J. L. McInnes, L. F. Chibotaru, R. E. P. Winpenny, *Nat. Chem*., 2013, **5**, 673; (c) S. Demir, J. M. Zadrozny, M. Nippe, J. R. Long, *J. Am. Chem. Soc*., 2012, **134**, 18546; (d) Y.-N. Guo, G.-F. Xu, W. Wernsdorfer, L. Ungur, Y. Guo, J. Tang, H.-J. Zhang, L. F. Chibotaru, A. K. Powell, *J. Am. Chem. Soc.*, 2011, **133**, 11948; (e) J. J. Le Roy, M. Jeletic, S. I. Gorelsky, I. Korobkov, L. Ungur, L. F. Chibotaru, M. Murugesu, *J. Am. Chem. Soc*., 2013, **135**, 3502; (f) J. Tang, I. Hewitt, N. T. Madhu, G. Chastanet, W. Wernsdorfer, C. E. Anson, C. Benelli, R. Sessoli, A. K. Powell, *Angew. Chem., Int. Ed*., 2006, **43**, 1729.

9 (a) E.; Coronado, C.; Giménez-Saiz, A.; Recuenco, A.; Tarazón, F. M.; Romero, A.; Camón, F. Luis, *Inorg. Chem*., 2011, **50**, 7370; (b) J. D. Rinehart, M. Fang, W. J. Evans, J. R. Long, *J. Am. Chem. Soc*., 2011, **133**, 14236; (c) N. Ishikawa, M. Sugita, W. Wernsdorfer, *Angew. Chem., Int. Ed*., 2005, **42**, 2931.

10 (a) R. A. Layfield, *Organometallics*, 2014, **33**, 1084; (b) V. Chandrasekhar, S. Das, A. Dey, S. Hossain, J.-P. Sutter, *Inorg.Chem.*, 2013, **52**, 11956.

11 (a) S.-D. Jiang, B.-W. Wang, H.-L. Sun, Z.-M. Wang, S. Gao, *J. Am. Chem. Soc.*, 2011, **133**, 4730; (b) A. Yamashita, A. Watanabe, S. Akine, T. Nabeshima, M. Nakano, T. Yamamura, T. Kajiwara, *Angew. Chem., Int. Ed*., 2011, **50**, 4016; (c) M. A. AlDamen, J. M. Clemente-Juan, E. Coronado, C. Martí-Gastaldo, A. Gaita-Ariño, *J. Am. Chem. Soc*., 2008, **130**, 8874; (d) P. Zhang, L. Zhang, C. Wang, S. Xue, S.-Y. Lin, J. Tang, *J. Am. Chem. Soc*., 2014, **136**, 4484.

12 (a) Sabbatini, N.; Guardigli, M.; Lehn, J.-M.*Coord. Chem. Rev*., 1993, **123**, 201; (b) L. Armelao, S. Quici, F. Barigelletti, G. Accorsi, G. Bottaro, M. Cavazzini, E. Tondello, *Coord. Chem. Rev*., 2010, **254**, 487.

13 (a) L. Bogani, L. Cavigli, M. Gurioli, R.; L. Novak, M. Mannini, A. Caneschi, F. Pineider, R. Sessoli, M. Clemente-León, E. Coronado, A. Cornia, D. Gatteschi, *Adv. Mater*., 2007, **19**, 3906; (b)

R. Moroni, R. Buzioa, A. Chincarini, U. Valbusaa, F. B. de Mongeot, L. Bogani, A. Caneschi, R. Sessoli, L. Cavigli, M. Gurioli, *J. Mater. Chem*., 2008, **18**, 109.

14 (a) L. Jerome. R. Vallat, R. A. S. Ferreira, L. D. Carlos, F. A. Almeida Paz, Y. Guari, J. Larionova, *Chem. Commun*., 2012, **48**, 9974; (b) A. B. Canaj, D. I. Tzimopoulos, A. Philippidis, G. E. Kostakis, C. J. Milios, *Inorg. Chem.*, 2012, **51**, 7451; (c) G. Cucinotta, M. Perfetti, J. Luzon, M. Etienne, P.- E. Car, A. Caneschi, G. Calvez, K. Bernot, R. Sessoli, *Angew. Chem., Int. Ed.,* 2012, **51**, 1606; (d) D. I. Alexandropoulos, A. Fournet, L. Cunha-Silva, A. M. Mowson, V. Bekiari, G. Christou, T. C. Stamatatos, *Inorg. Chem*., 2014, **53**, 5420; (e) S. Mohapatra, B. Rajeswaran, A. Chakraborty, A. Sundaresan, T. K. Maji, *Chem. Mater*., 2013, **25**, 1673.

15 V. Chandrasekhar, P. Bag, M. Speldrich, J. van-Leusen, P. Kögerler, *Inorg.Chem*., 2013, **52**, 5035.

16 B. S. Furniss, A. J. Hannaford, P. W. G. Smith, A. R. Tatchell, *Vogel's Text book of Practical Organic Chemistry*, *5th edition*, ELBS, Longman: London, 1989.

17 C. A. Paeker, W. T. Ress, *Analyst*., 1960, **85**, 587.

18 J. Olmsted, *J. Phys. Chem*., 1979, **83**, 2581.

19 (a) SMART & SAINT *Software Reference manuals*, version 6.45; Bruker Analytical X-ray Systems, Inc.: Madison, WI, 2003; (b) G. M. Sheldrick, SADABS, *a software for empirical absorption correction*; version 2.05; University of Göttingen: Göttingen, Germany, 2002; (c) SHELXTL *Reference Manual*, version 6.1; Bruker Analytical X-ray Systems, Inc.: Madison, WI, 2000; (d) G. M. Sheldrick, *SHELXT*, version 6.12; Bruker AXS Inc.: Madison, WI, 2001; (e) G. M. Sheldrick, SHELXL97, *Program for Crystal Structure Refinement*; University of Göttingen: Göttingen, Germany, 1997; (f) K. Brandenburg, *Diamond*, v3.1e; Crystal Impact GbR: Bonn, Germany, 2005.

20 (a) S. Schmidt, D. Prodius, G. Novitchi, V. Mereacre, G. E. Kostakis, A. K. Powell, *Chem. Commun.*, 2012, **48**, 9825; (b) M. Li, Y. Lan, A. M. Ako, W. Wernsdorfer, C. E. Anson, G. Buth, A. K. Powell, Z. Wang, S. Gao, *Inorg. Chem.*, 2010, **49**, 11587; (c) S. K. Langley, N. F. Chilton, B. Moubaraki, K. S. Murray, *Dalton Trans*., 2012, **41**, 1033.

21 (a) E. E. S. Teotonio, H. F. Brito, M. C. F. C. Felinto, L. C. Thompson, V. G. Young, O. L. Malta, *J. Mol. Struct*., 2005, **751**, 85; (b) G. B. Deacon, R. Phillips, *J. Coord. Chem. Rev.*, 1980, **33**, 227.

22 (a) X. Yi, K. Bernot, F. Pointillart, G. Poneti, G. Calvez, C. Daiguebonne, O. Guillou, R. Sessoli, *Chem.-Eur. J.*, 2012, **18**, 11379; (b) Y. Guo, G. Xu, W. Wernsdorfer, L. Ungur, Y. Guo, J. Tang, H. Zhang, L. F. Chibotaru, A. K. Powell, *J. Am. Chem. Soc*., 2011, **133**, 11948; (c) J. Long, F. Habib, P. H. Lin, I. Korobkov, G. Enright, L. Ungur, W. Wernsdorfer, L. F. Chibotaru, M. Murugesu, *J. Am. Chem. Soc*., 2011, **133**, 5319; (d) Y. Guo, X. Chen, S. Xue, J. Tang, *Inorg. Chem*., 2011, **50**, 9705; (e) P. –H. Lin, T. J. Burchell, R. Clerac, M. Murugesu, *Angew. Chem. Int. Ed*., 2008, **47**, 8848.

23 V. Chandrasekhar, P. Bag, B. Murugesapandian, M. D. Pandey, *Dalton Trans*., 2013, **42**, 15447.

24 (a) Y. Bi, X.-T. Wang, W. Liao, X. Wang, R. Deng, H. Zhang, S. Gao, *Inorg. Chem*., 2009, **48**, 11743; (b) A. B. Canaj, D. I. Tzimopoulos, A. Philippidis, G. E. Kostakis, C. J. Milios, *Inorg. Chem.* 2012, **51**, 7451; (c) S. Biju, N. Gopakumar, J.-C. G. Bünzli, R. Scopelliti, H. K. Kim, M. L. P. Reddy, *Inorg.Chem*., 2013, **52**, 875.

25 (a) G. H. Dieke, *Spectra and Energy levels of Rare Earth Ions in Crystals*; Interscience: New York, 1968; (b) S. Biju, M. L. P. Reddy, A. H. Cowley, K. V. Vasudevan, *J. Mater. Chem*., 2009, **19**, 5179; (c) A. P. S. Samuel, E. G. Moore, M. Melchior, J. Xu, K. N. Raymond, *Inorg. Chem*., 2008, **47**, 7535.

26 M. Latva, H. Takalo, V. M. Mukkala, C. Matachescu, J. C. Rodriguez-Ubis, J. Kanakare, *J. Lumin.*, 1997, **75**, 149.

27 Lewis, D. J.; Glover, B. G.; Solomons, M. C.; Pikramenou, Z. *J. Am. Chem. Soc*. **2011**, *133*, 1033.

28 R. E. Whan, G. A. Crosby, *J. Mol. Spectrosc*., 1962, **8**, 315.

29 G. A. Crosby, R. E. Whan, R. M. Alire, *J. Chem. Phys*., 1961, **34**, 743.

30 (a) J.V. Caspar, T. J. Meyer, *J. Am. Chem. Soc.*, 1983, **105**, 5583; (b) A. P. S. Samuel, E. G. Moore, M. Melchior, J. Xu, K. N. Raymond, *Inorg. Chem*.; 2008, **47**, 7535.

31 F. J. Steemers, W. Verboom, D. N. Reinhoudt, E. B. Vander Tol, J. W. Verhoeven, *J. Am. Chem. Soc.*, 1995, **117**, 9408.

32 (a) P. Froidevaux, J.-C. G. Bunzli, *J. Phys. Chem*., 1994, **98**, 532; (b) S.; Sivakumar, M. L. P. Reddy, A. H. Cowley, K. V. Vasudevan, *Dalton Trans*., 2010, **39**, 776.

33 (a) F. R. Goncalves e Silva, R. Longo, O. L. Malta, C. Piguet, J.-C. G. Bünzli, *Phys. Chem. Chem. Phys*., **2000**, **2**, 5400; (b) J.-C. G. Bünzli, P. Froidevaux, J. M. Harrowfield, *Inorg. Chem*., 1993, **32**, 3306; (c) A. Beeby, S. Faulkner, D. Parker, J. A. Gareth Williams, *J. Chem. Soc., Perkin Trans*., 2001, **2**, 1268.

34 (a) C. Benelli, D. Gatteschi, *Chem. Rev*., 2002, **102**, 2369; (b) J.-P. Sutter, M. L. Kahn, *Magnetism: Molecules to Materials*; J. S. Miller, M. Drillon, Eds.;Wiley-VCH: Weinheim, Germany, 2005, Vol. 5, pp 161– 188.

35 (a) J.-P. Sutter, M. L. Kahn, O. Kahn, *Adv. Mater*., 1999, **11**, 863; (b) M. L. Kahn, J.-P. Sutter, S. Golhen, P. Guionneau, L. Ouahab, O. Kahn, D. Chasseau, *J. Am. Chem. Soc*., 2000, **122**, 3413; (c) D. I. Alexandropoulos, L. Cunha-Silva, L. Pham, V. Bekiari, G. Christou, T. C. Stamatatos, *Inorg. Chem.*, 2014, **53**, 3220.

36 (a) J.-P. Costes, J. -M. C. Juan, F. Dahan, F. Nicodéme, *Dalton Trans*., 2003, 1272; (b) V. Chandrasekhar, P. Bag, E. Colacio, *Inorg. Chem*., 2013, **52**, 4562; (c) F. Avecilla, C. Platas-Iglesias, R. Rodríguez-Cortiñas, G. Guillemot, J.C. G. Bünzli, C. D. Brondino, C. F. G. C. Geraldes, A. de Blas, T. *J.* Rodríguez-Blas, *Chem. Soc. Dalton Trans*., 2002, 4658.

37 (a) E. Colacio, J. Ruiz, A. J. Mota, M. A. Palacios, E. Cremades, E. Ruiz, F. J. White, E. K. Brechin, *Inorg. Chem*., 2012, **51**, 5857; (b) S. Das, A. Dey, S. Biswas, E. Colacio, V. Chandrasekhar, *Inorg. Chem*., 2014, **53**, 3417.

38 (a) Y.-N. Guo, G.-F. Xu, P. Gamez, L. Zhao, S.-Y. Lin, R. Deng, J. Tang, H.-J. Zhang, *J. Am. Chem. Soc*., 2010, **132**, 8538; (b) Y. Miyashita, M. Sanada, M. M. Islam, N. Amir, T. Koyano, H. Ikeda, K. Fujisawa, K. Okamoto, *Inorg. Chem. Commun*., 2005, **8**, 785; (c) H. Ke, G.-F. Xu, Y.-N. Guo, P. Gamez, C. M. Beavers, S. J. Teat, J. Tang, *Chem. Commun*., 2010, **46**, 6057.

39 (a) J. Ruiz, A. J. Mota, A. Rodriguez-Dieguez, S. Titos, J. M. Herrera, E. Ruiz, E. Cremades, J. P. Costes, E. Colacio, *Chem. Commun*., 2012, **48**, 7916; (b) Cuccinota, G.; Perfetti, M.; Luzon, J.; Etienne, M.; Car, P.-E.; Caneschi, A.; Calvez, G.; Bernot, K.; Sessoli, R. *Angew. Chem., Int. Ed.*, **2012**, *51*, 1606; (c) K. R. Meihaus, J. R. Rinehart, J. R. Long, *Inorg. Chem*., 2011, **50**, 8484.

40 (a) S. D. Jiang, S. -S. Liu, L. -N. Zhou, B. W. Wang, Z. M. Wang, S. Gao, *Inorg. Chem.*, 2012, **51**, 3079; (c) K. R. Meihaus, J. R. Rinehart, J. R. Long, *Inorg. Chem.*, 2011, **50**, 8484.

41 K. S. Cole, R. H. Cole, *J. Chem. Phys*., 1941, **9**, 341.

Synopsis

Homodinuclear Lanthanide {Ln_2} (Ln = Gd, Tb, Dy, Eu) Complexes Prepared from *o*-Vanillin based Ligand: Luminescence and Single-Molecule Magnetism Behavior

Prasenjit Bag,[a] Chandresh Kumar Rastogi,[b] Sourav Biswas,[a] Sri Sivakumar,[b,c] Valeriu Mereacre*[d] Vadapalli Chandrasekhar,*[a,e]*

The reaction of a multisite coordination ligand (LH_3) with Ln(III) chloride salts in presence of in presence of pivalic acid and triethylamine as base afforded a series of homometallic dinuclear neutral complexes [Gd_2 $(LH_2)_2$ (μ-piv)$_2$ (piv)$_2$]2$CHCl_3$ {Ln = Gd(**1**), Tb(**2**), Dy(**3**), Eu(**4**)} complexes. The details of photophysical and magnetic property study shows that Tb^{3+} (**2**) and Dy^{3+} (**3**) complexes display ligand sensitized strong lanthanide characteristic emission with concomitant appearance of single molecule magnet behavior in Dy^{3+} (**3**) complex.

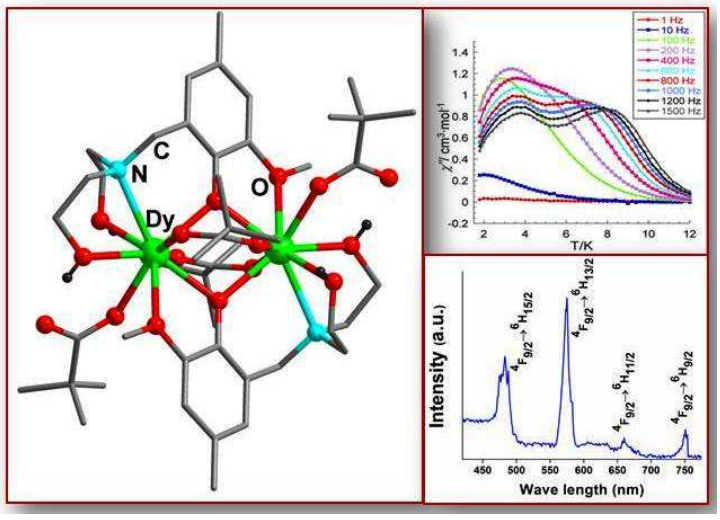

Supplementary Information

Homodinuclear Lanthanide {Ln_2} (Ln = Gd, Tb, Dy, Eu) Complexes Prepared from *o*-Vanillin based Ligand: Luminescence and Single-Molecule Magnetism Behavior

Prasenjit Bag,[a] Chandresh Kumar Rastogi,[b] Sourav Biswas,[a] Sri Sivakumar,[b,c] Valeriu Mereacre*[d] Vadapalli Chandrasekhar,*[a,e]*

[a]Department of Chemistry, Indian Institute of Technology Kanpur, Kanpur-208016, India,

[b]Material Science Programme, Indian Institute of Technology Kanpur, Kanpur, India.

[c]Department of Chemical Engineering and Centre for Environmental Science and Engineering, Indian Institute of Technology Kanpur, Kanpur, India.

[d]Institute of Inorganic Chemistry, Karlsruhe Institute of Technology, Engesserstrasse 15, 76128 Karlsruhe, Germany.

[e]National Institute of Science Education and Research, Institute of Physics Campus, Sachivalaya Marg, Sainik School Road, Bhubaneshwar-751 005, Odisha, India

AUTHOR EMAIL ADDRESS: vc@iitk.ac.in; srisiva@iitk.ac.in

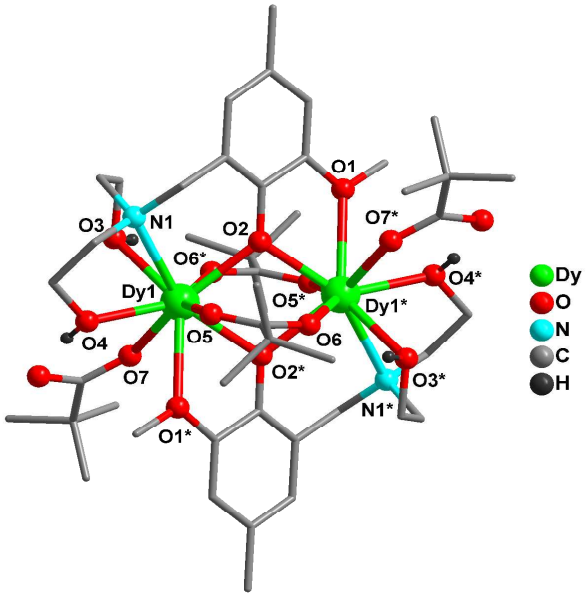

Fig. S1 Molecular structure of **3 (**hydrogen atoms and solvent molecules are omitted for clarity).

Table S1. Selected Bond distances and bond angles for compound **3**

Bond lengths (Å)		Bond angles (°)	
Bond Lengths around Dysprosium(1)			
Dy(1)-O(2)*	2.305(3)	O(2)-Dy(1)-O(3)	96.43(9)
Dy(1)-O(2)	2.337(3)	O(2)*-Dy(1)-O(4)	133.63(9)
Dy(1)-O(7)	2.338(3)	Dy(1)*-O(2)-Dy(1)	103.02(10)
Dy(1)-O(5)	2.344(3)	O(2)-Dy(1)-O(1)*	126.01(9)
Dy(1)-O(4)	2.361(3)		
Dy(1)-O(6)*	2.472(3)		
Dy(1)-O(3)	2.524(3)		
Dy(1)-O(1)*	2.675(3)		
Dy(1)-N(1)	2.679(3)		
Dy(1)-Dy(1)*	3.6331(13)		

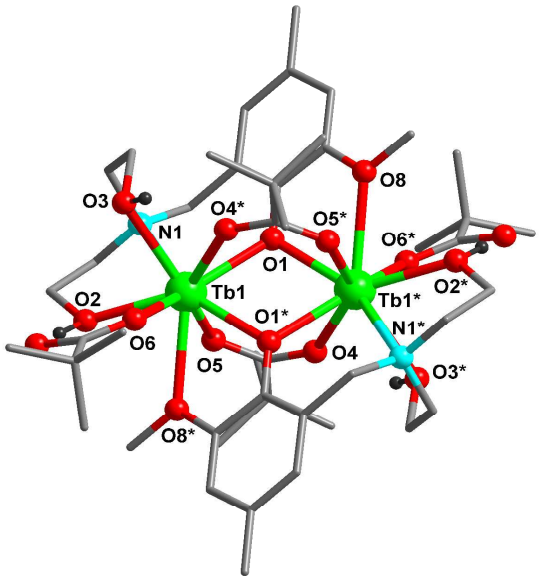

Fig. S2 Molecular structure of **2 (**hydrogen atoms and solvent molecules are omitted for clarity).

Table S2. Selected Bond distances and bond angles for compound **2**

Bond lengths (Å)		Bond angles (°)	
Bond Lengths around Terbium(1)			
Tb(1)-O(5)	2.365(3)	O(2)-Dy(1)-O(3)	96.43(9)
Tb(1)-O(6)	2.351(3)	O(2)*-Dy(1)-O(4)	133.63(9)
O(8)*-Tb(1)	2.677(3)	Dy(1)*-O(2)-Dy(1)	103.02(10)
Tb(1)-O(1)*	2.348(3)	O(2)-Dy(1)-O(1)*	126.01(9)
Tb(1)-O(2)	2.378(3)		
Tb(1)-O(4)*	2.474(3)		
Tb(1)-O(3)	2.538(3)		
Tb(1)-N(1)	2.682(3)		
Tb(1)-Tb(1)*	3.6532(14)		

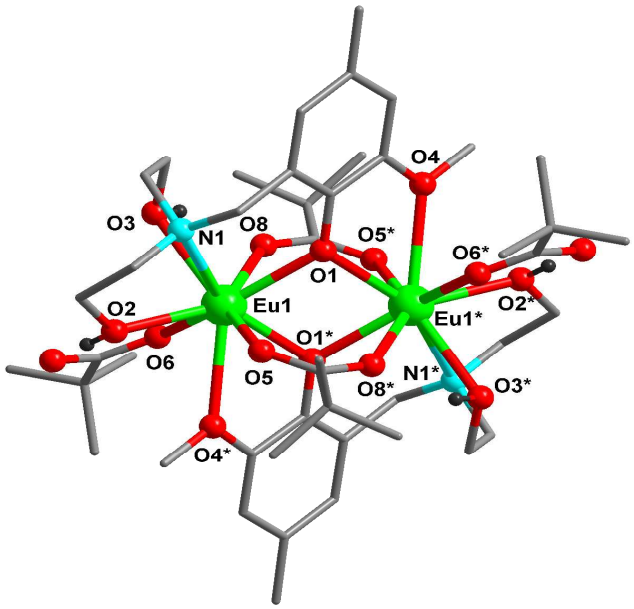

Fig. S3 Molecular structure of **4 (**hydrogen atoms and solvent molecules are omitted for clarity).

Table S3. Selected Bond distances and bond angles for compound **4**

Bond lengths (Å)		Bond angles (°)	
Bond Lengths around Europium(1)		Eu(1)*-O(1)-Eu(1)	102.76(12)
Eu(1)-O(1)	2.340(3)	O(1)*-Eu(1)-O(6)	85.00(11)
Eu(1)-O(1)	2.372(3)	O(1)-Eu(1)-N(1)	75.20(11)
Eu(1)-O(6)	2.378(3)	O(1)-Eu(1)-O(6)	143.63(11)
Eu(1)-O(5)	2.394(3)	O(6)-Eu(1)-O(5)	135.56(11)
Eu(1)-O(2)	2.401(3)		
Eu(1)-O(8)*	2.493(3)		
Eu(1)-O(3)	2.561(3)		
Eu(1)-O(4)*	2.674(3)		
Eu(1)-N(1)	2.704(4)		
Eu(1)-Eu(1)*	3.6816(6)		

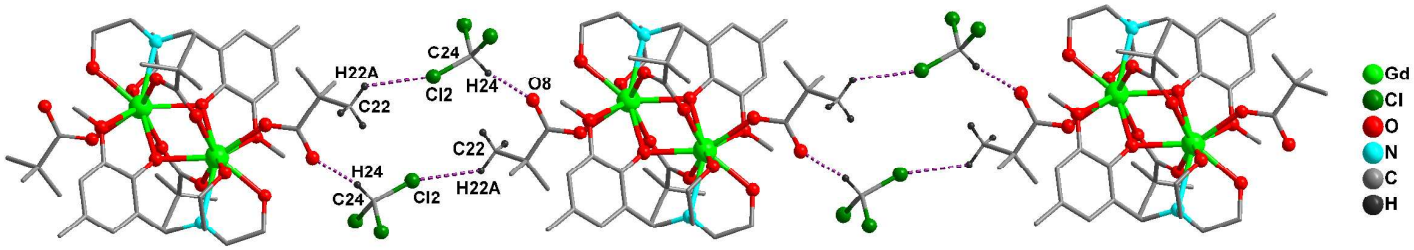

Fig. S4 1D polymeric supramolecular association through C-H…Cl and C-H…O hydrogen bonding of compound **1**.

Table S4. Hydrogen bond parameters for compound **1**

	D-H….A	d(D-H) Å	d(H….A) Å	d(D….A) Å	<(DHA)°	Symmetry of A
1	C22-H22A….Cl2	0.958(5)	2.885(2)	3.556(5)	128.99(28)	1-x, 0.5+y, 1.5-z
	C24-H24….O8	0.979(4)	2.026(4)	2.975(5)	158.02(25)	1-x, 3-y, 1-z

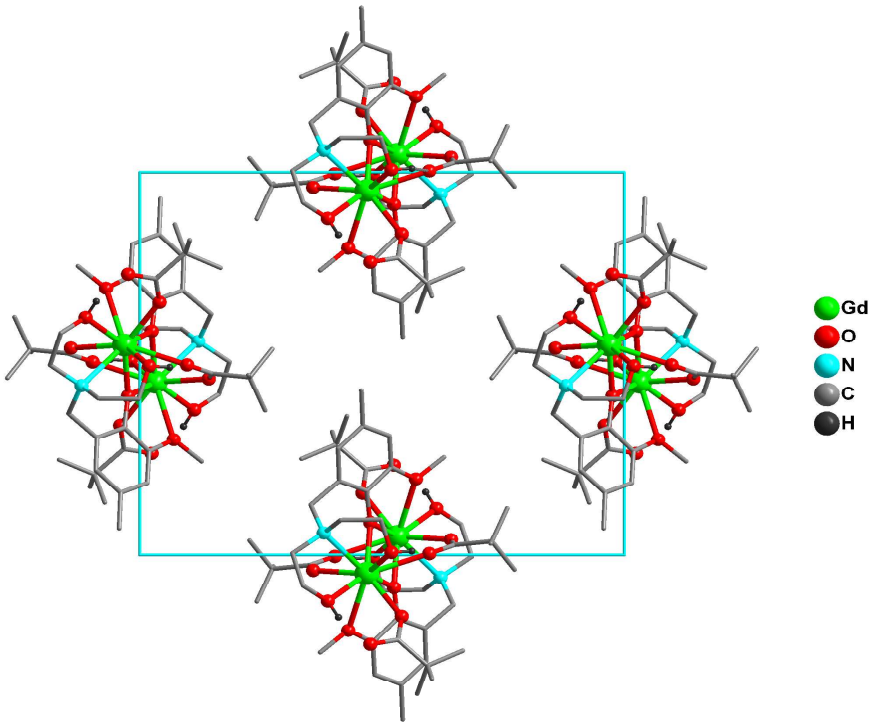

Fig. S5 Packing diagram compound **1.**

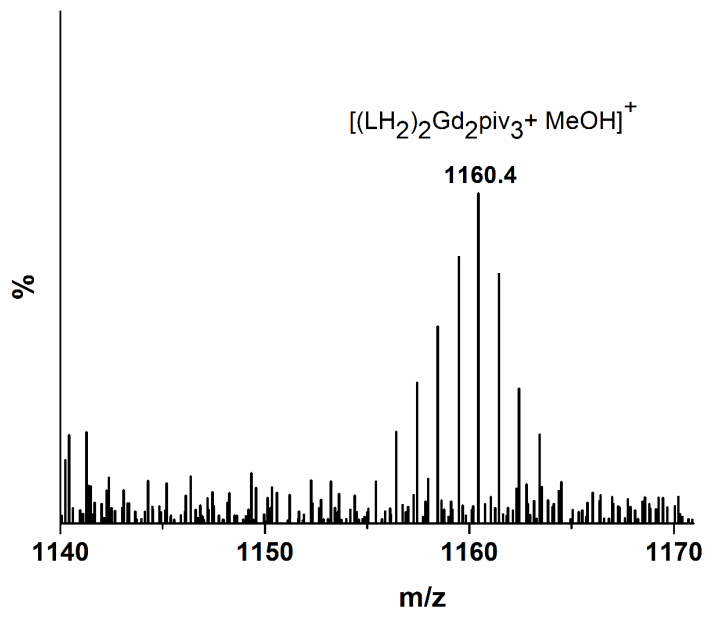

Fig. S6 ESI-MS of **1** (picture shows isotopic distribution pattern of one fragment).

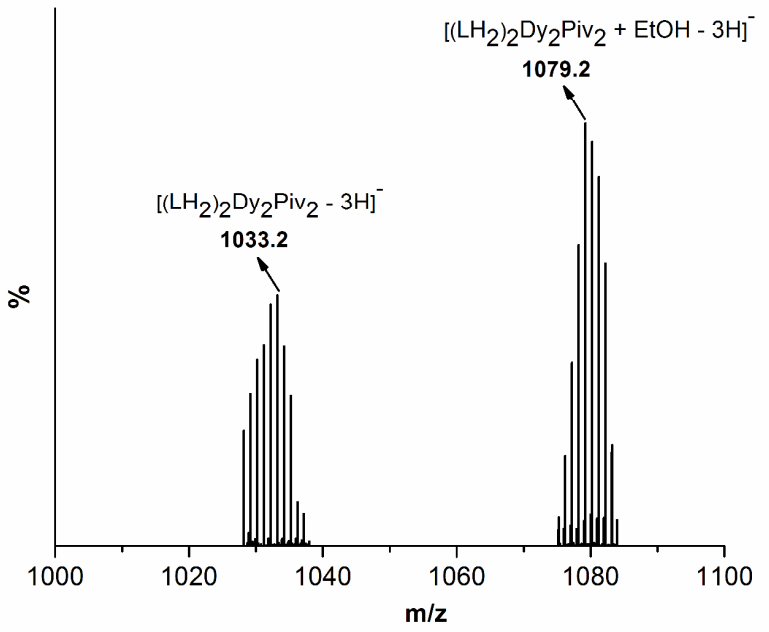

Fig. S7 ESI-MS of **3** (picture shows isotopic distribution pattern of the two fragments)

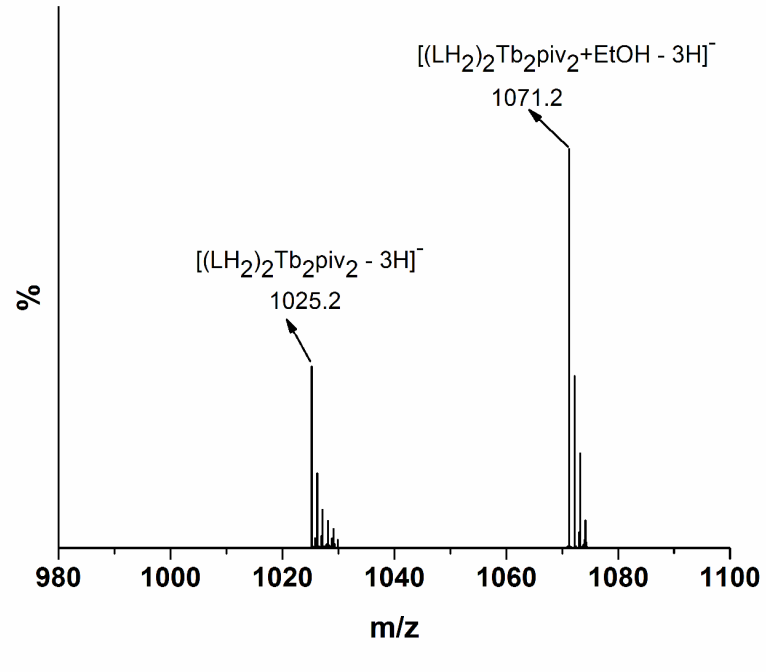

Fig. S8 ESI-MS of **2** (picture shows isotopic distribution pattern of the two fragments)

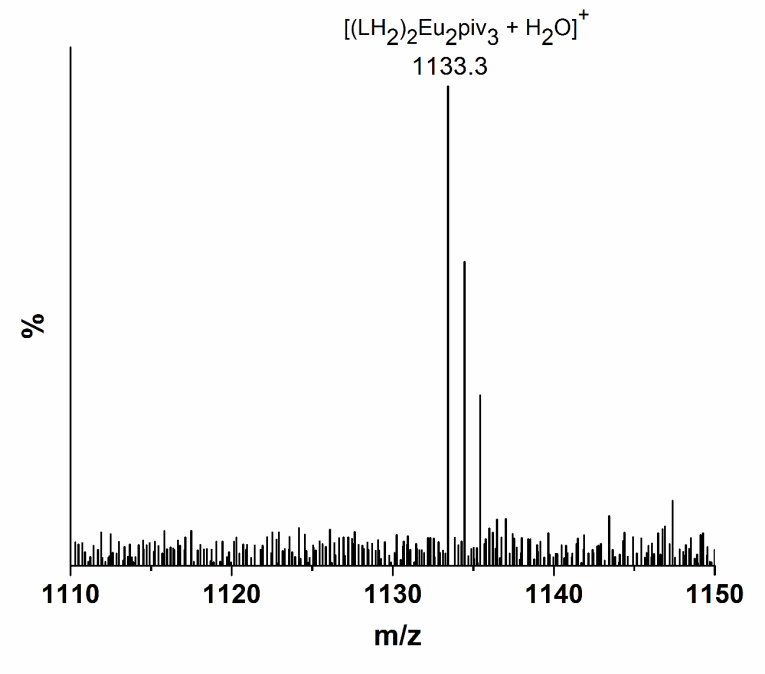

Fig. S9 ESI-MS of **4** (picture shows isotopic distribution pattern of one fragment).

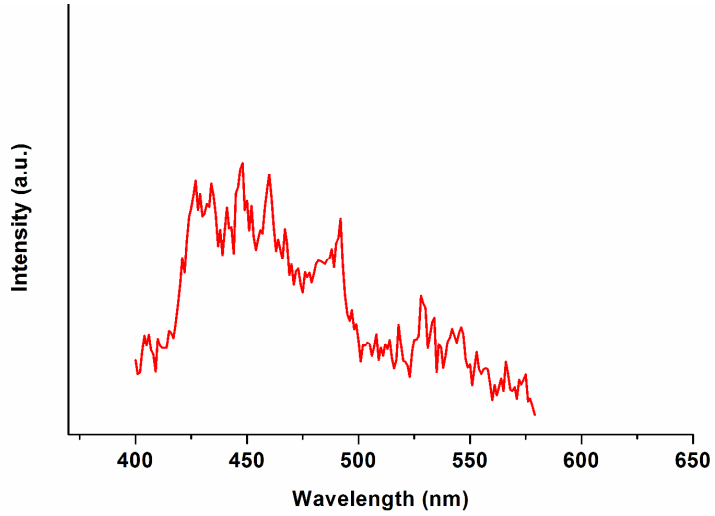

Fig. S10 Emission spectra of **4** (Eu_2) upon excitation at 300 nm.

Table S5. Life time of the complex **4**

Complex	Room Temperature Life time (τ_a) (μs), λ_{ex} = 300 (nm), λ_{em} = 450 (nm)
4	1.38

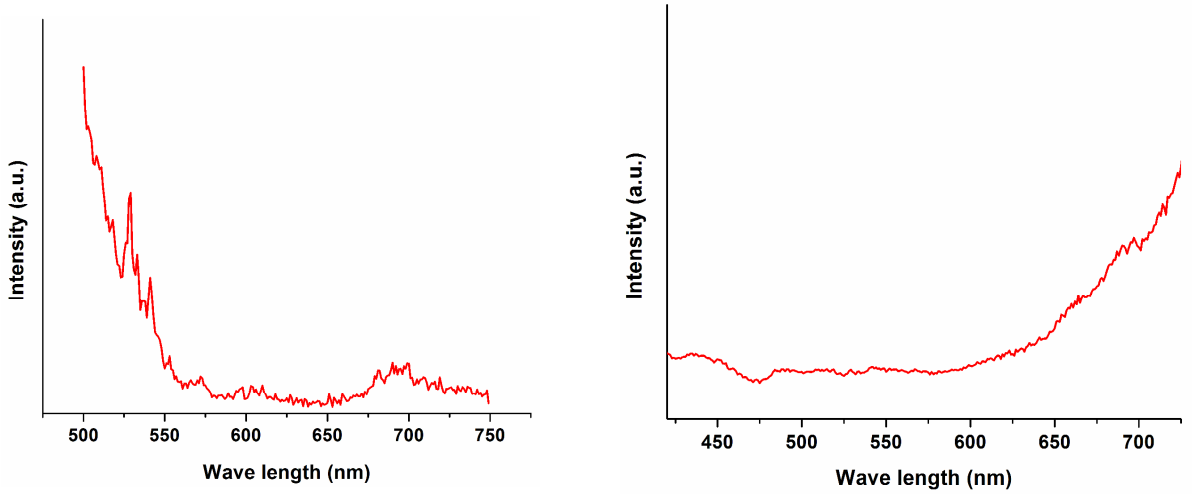

(a) (b)

Fig. S11 Emission spectra of **4** (Eu_2) upon excitation directly through the *f-f* transitions at (a) 464 nm and (b) 395 nm.

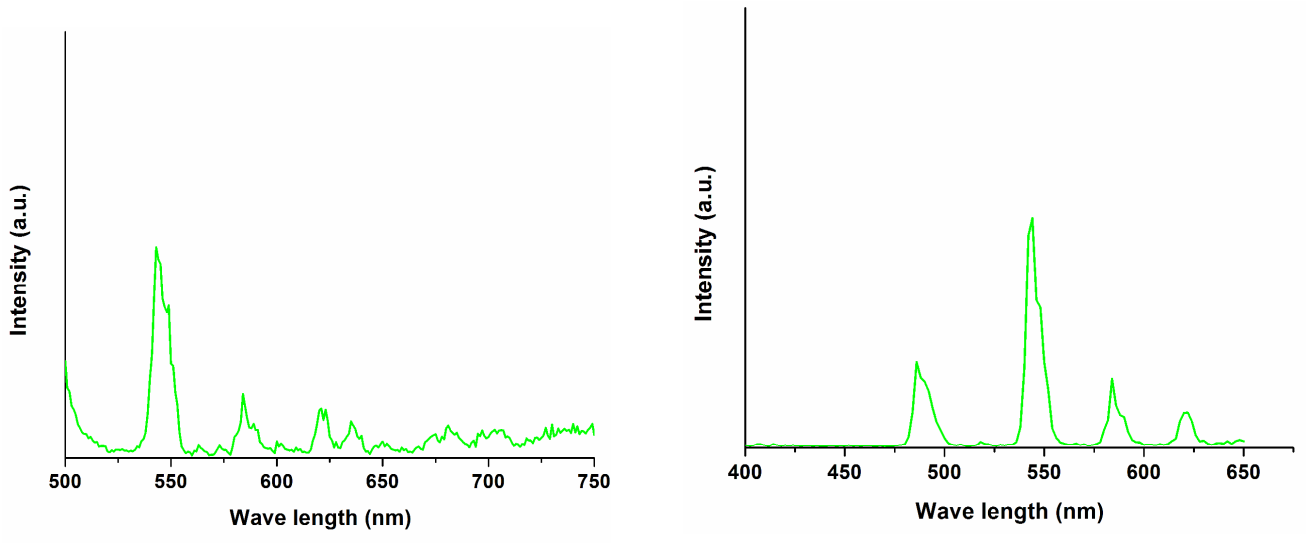

(a) (b)

Fig. S12 Emission spectra of **2** (Tb_2) upon excitation directly through the *f-f* transitions at (a) 488 nm and (b) 355 nm.

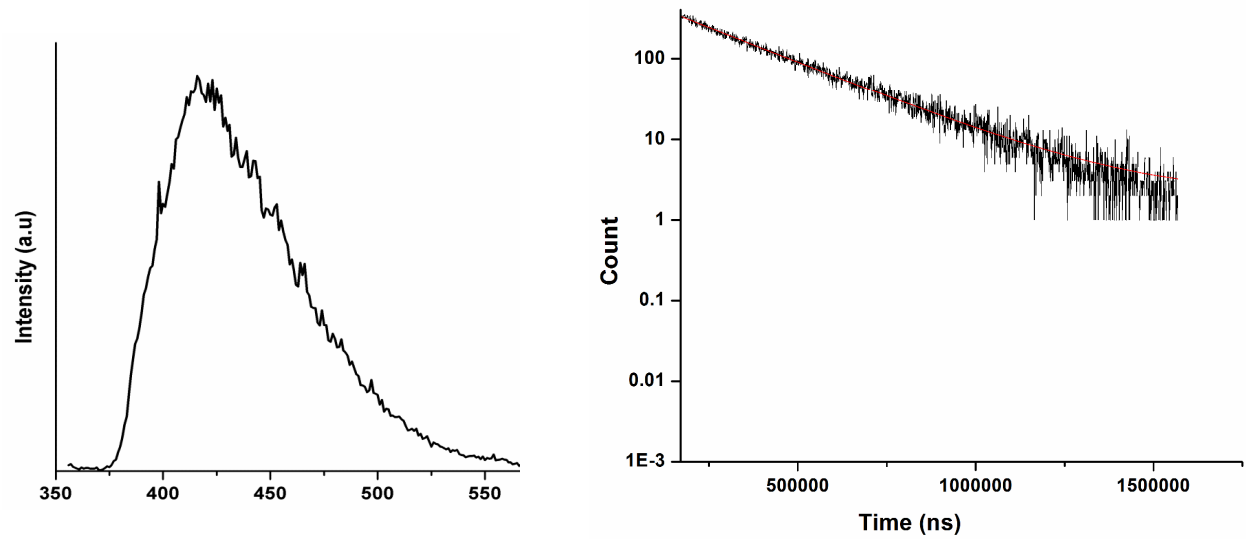

(a) (b)

Fig. S13 Room temperature (298 K) (a) phosphorescence spectra and (b) life time decay profile of Gd_2 (**1**) compound (λ_{ex} = 300 nm). The emission was monitored at 410 nm (The solid red line represent monoexponential fit to the decay curve with a τ value 250 μs.

Table S5. Life time of the ligand in presence and absence of acceptor.

Complex	Room Temperature Life time (τ_a) (μs), λ_{ex} = 300 (nm)	Room Temperature Life time (τ_0) (μs), λ_{ex} = 300 (nm)
1	-	250.33
2	1.66,	-
3	1.51	-

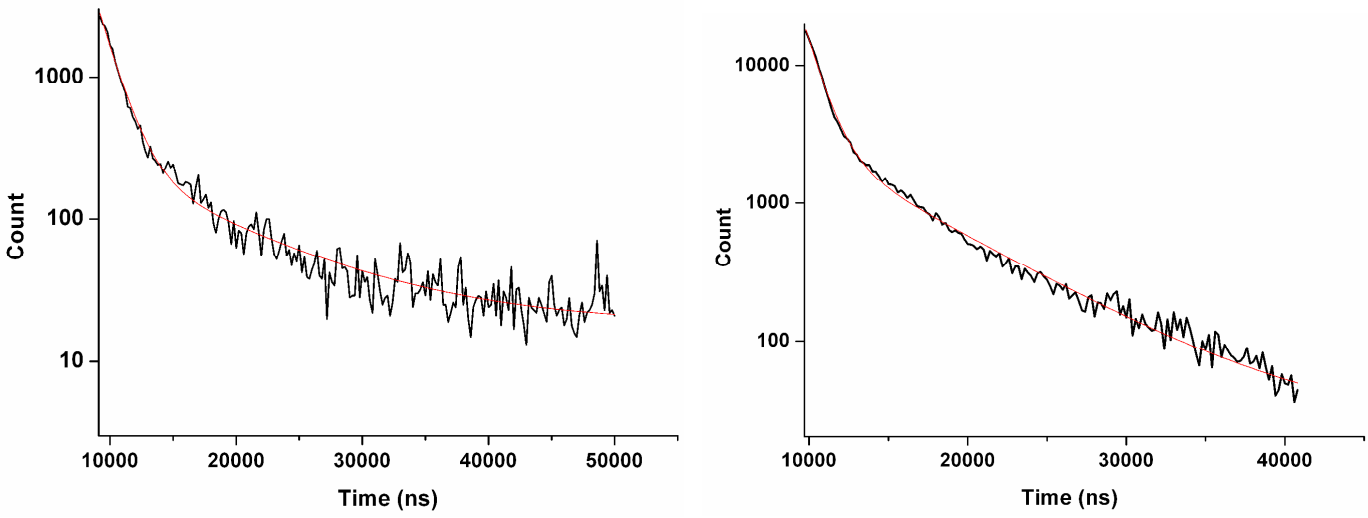

(a) (b)

Fig. S14 Phosphorescence decay profile (blue curve) of compounds **2** (a) and **3** (b) (λ_{ex} = 300 nm and emission monitored at 410 nm (ligand emission). The solid red line represents biexponential fit to the decay curve

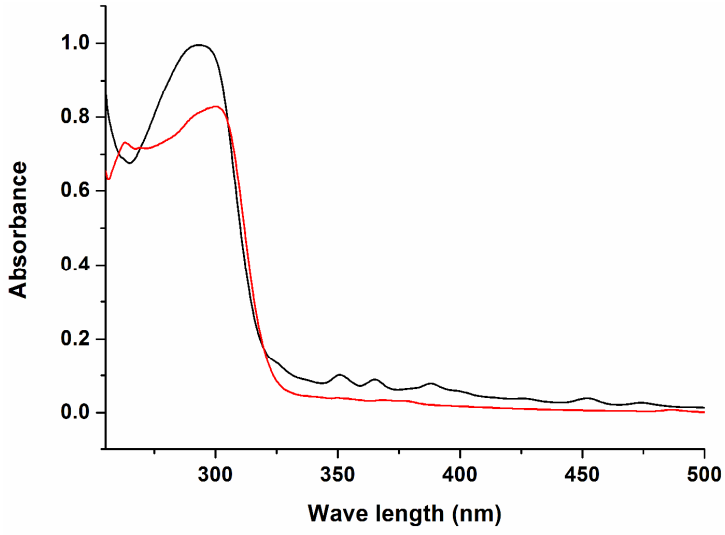

Fig. S15 Solid state absorption spectra of **2** (Tb_2, red line), **3** (Dy_2, black line).

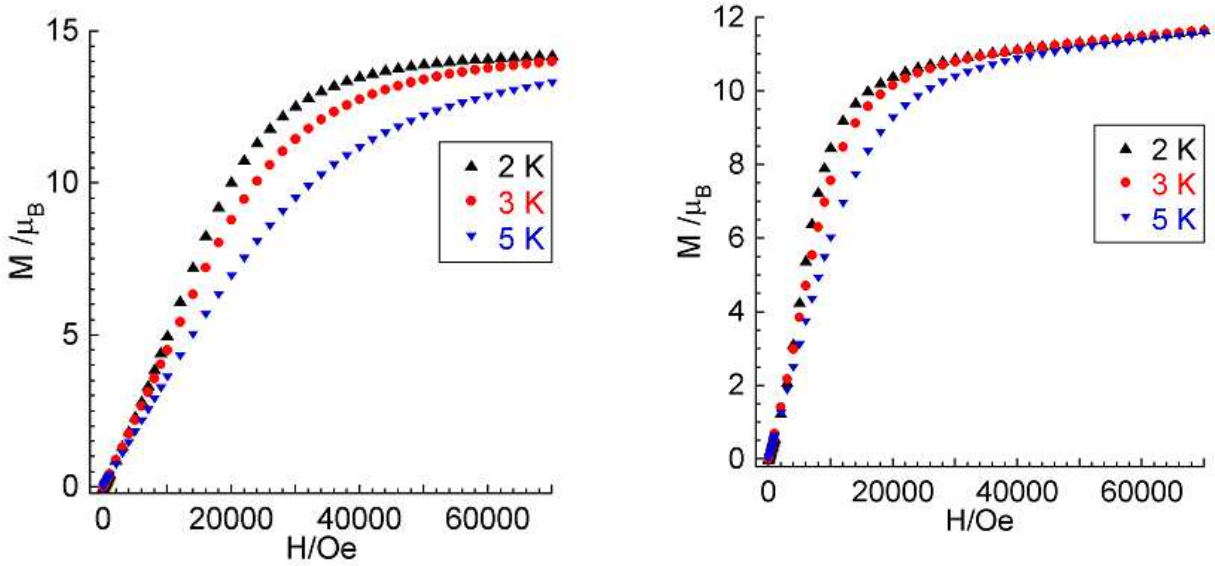

(a) (b)

Fig. S16 M versus H plot at 2, 3 and 5 K for compound **1** (a), **3** (b)

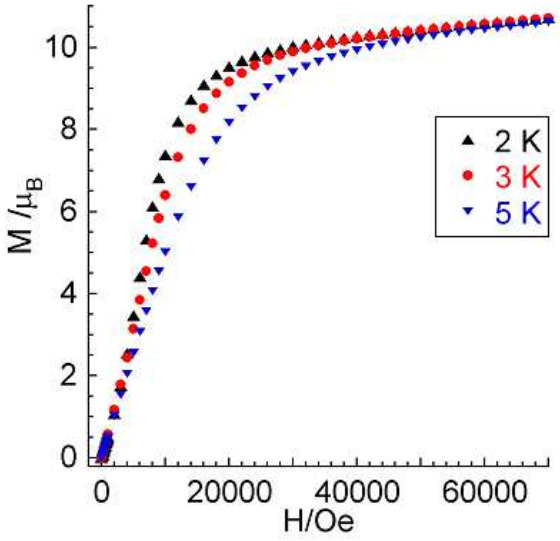

Fig. S17 M versus H plot at 2, 3 and 5 K for compound **2**

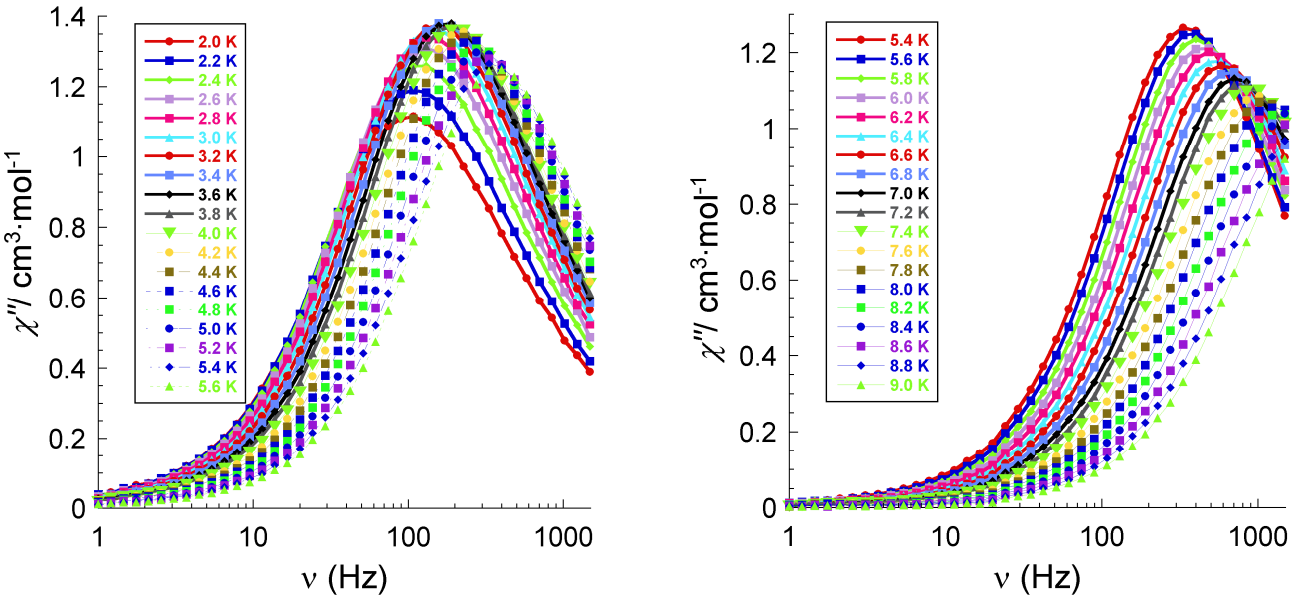

(a) (b)

Fig. 18 Frequency dependent of the out-of-phase ac signals (χ''_M) under zero applied dc field for **3** at low temperature (a) and at high temperature (b) region. Solid lines are a guide to the eye.

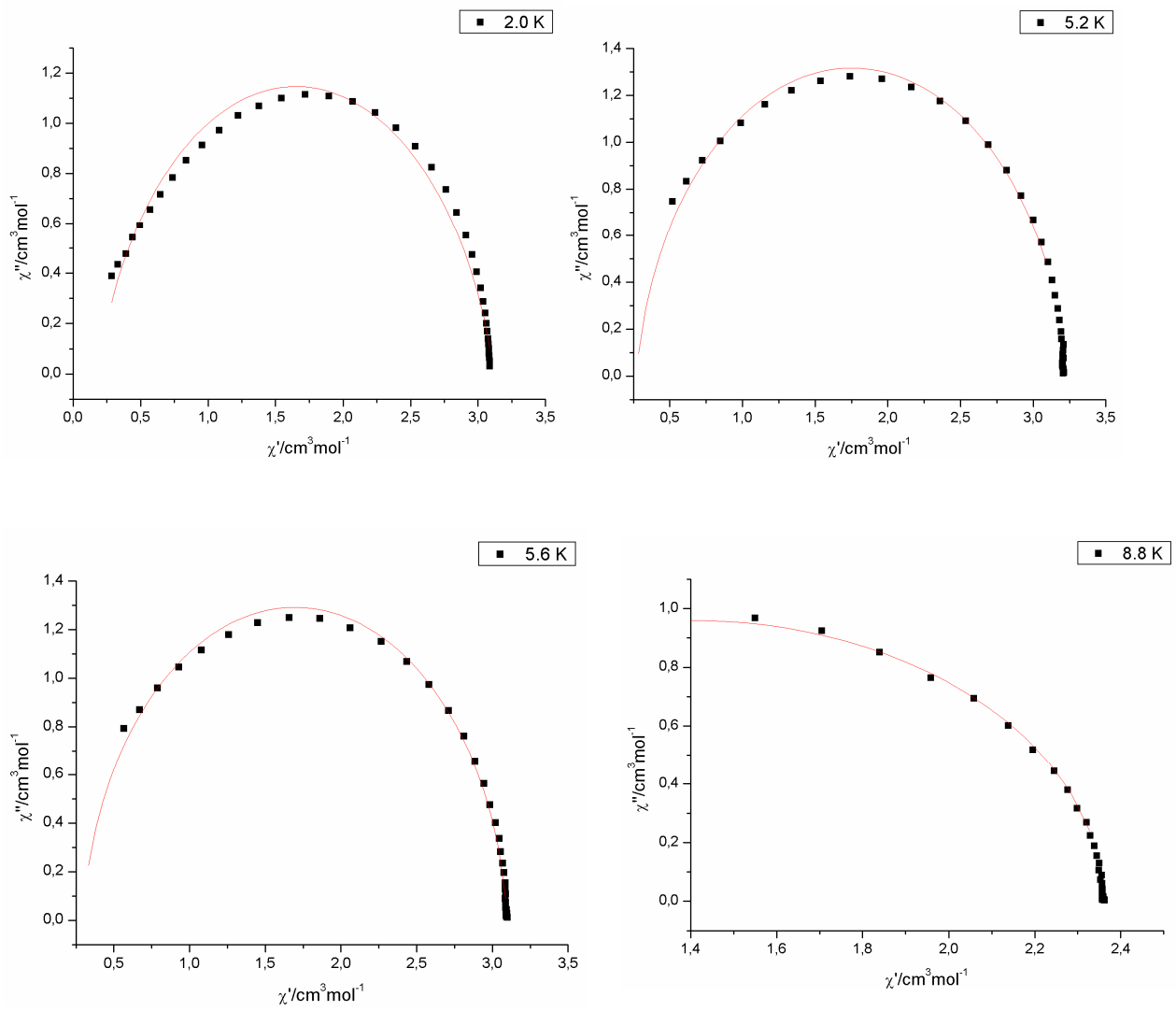

Fig. S19 Cole-Cole plot using the ac susceptibility data shown in Fig. S18 for **3**. The solid lines are the best fit obtained with a generalized Debye model (with α always smaller than 0.15).

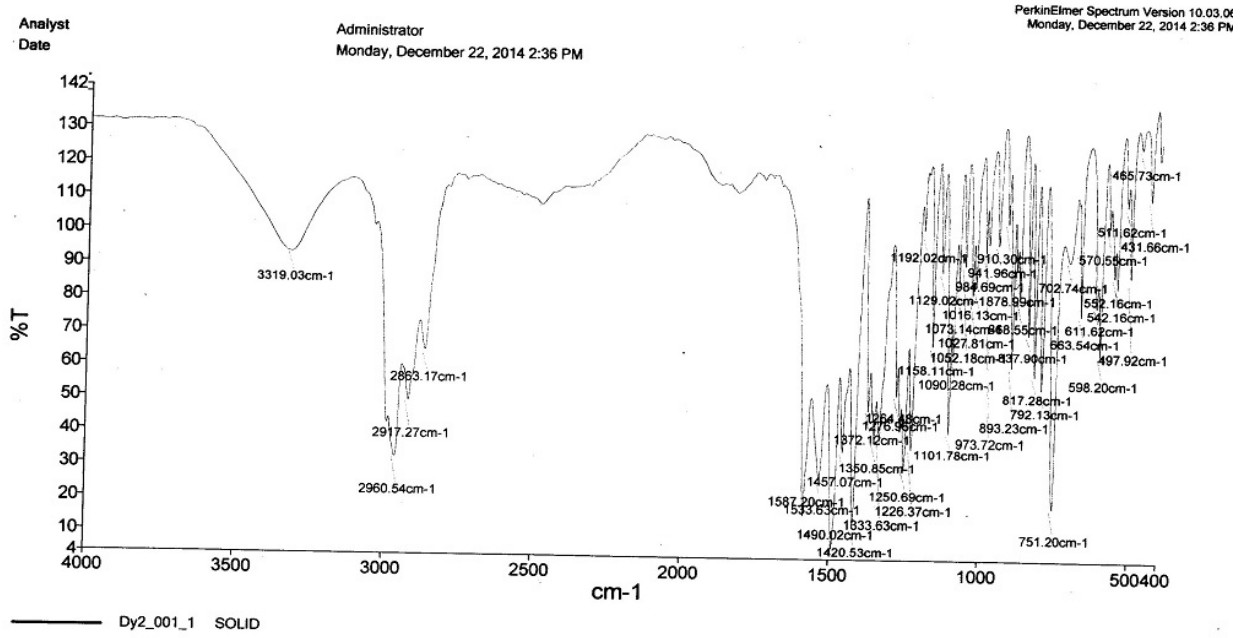

Fig. S20 IR spectra of compound **3** (Dy_2)

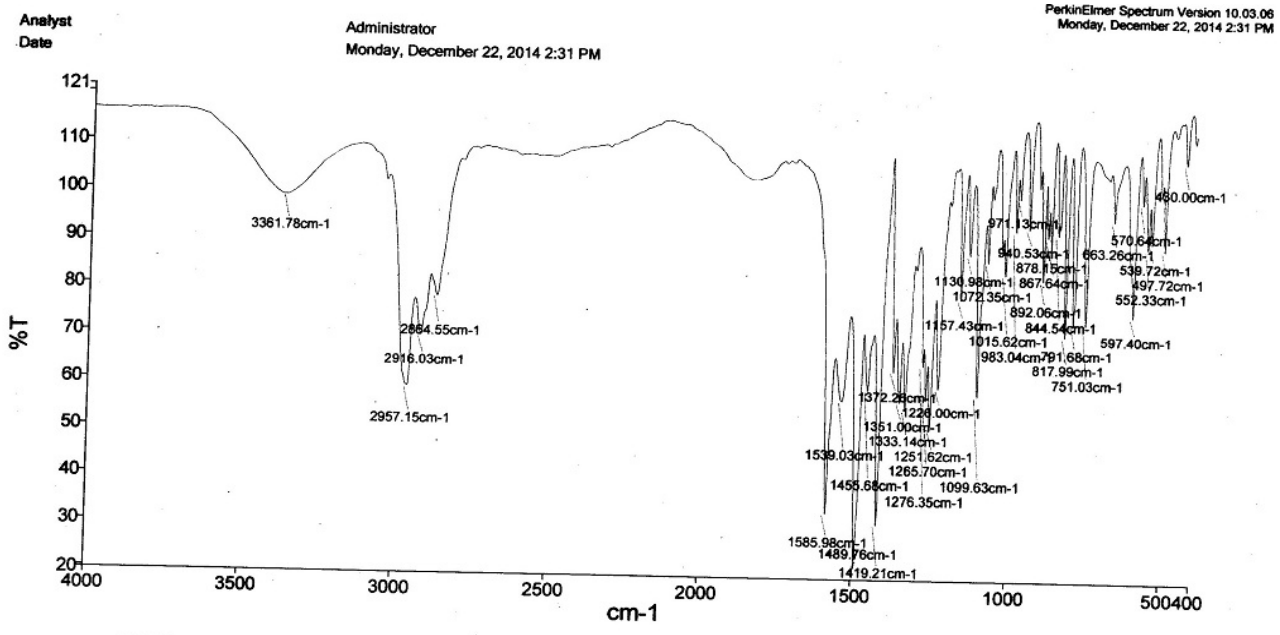

Fig. S21 IR spectra of compound **1** (Gd_2)

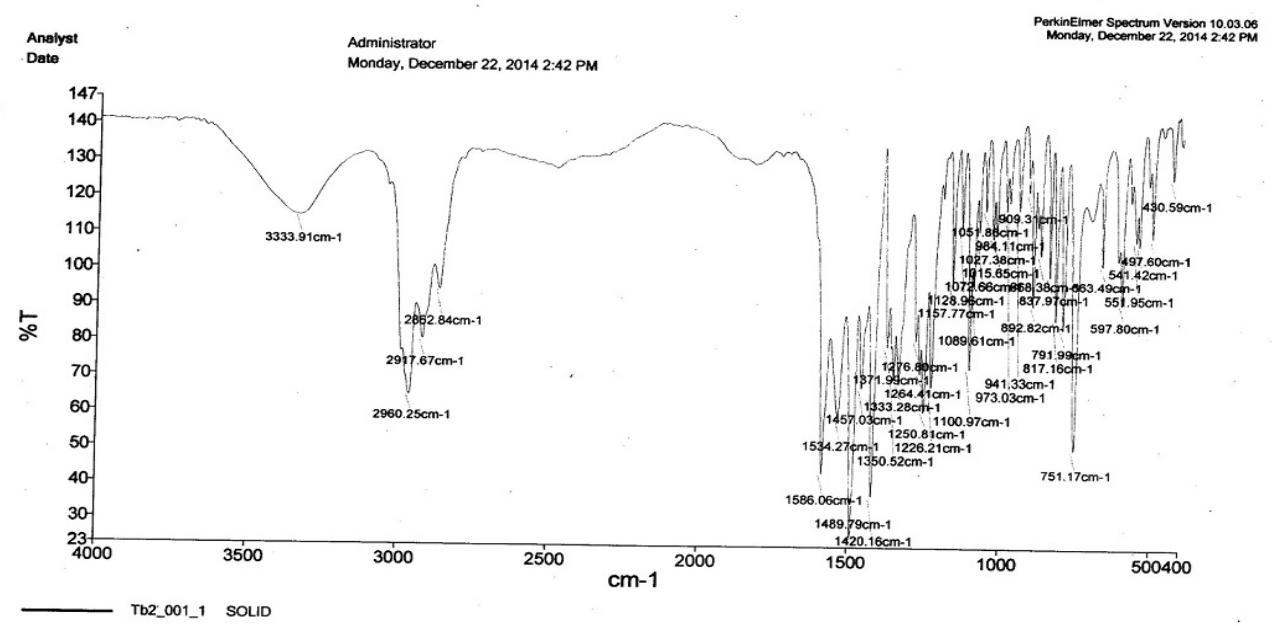

Fig. S22 IR spectra of compound **2** (Tb_2).

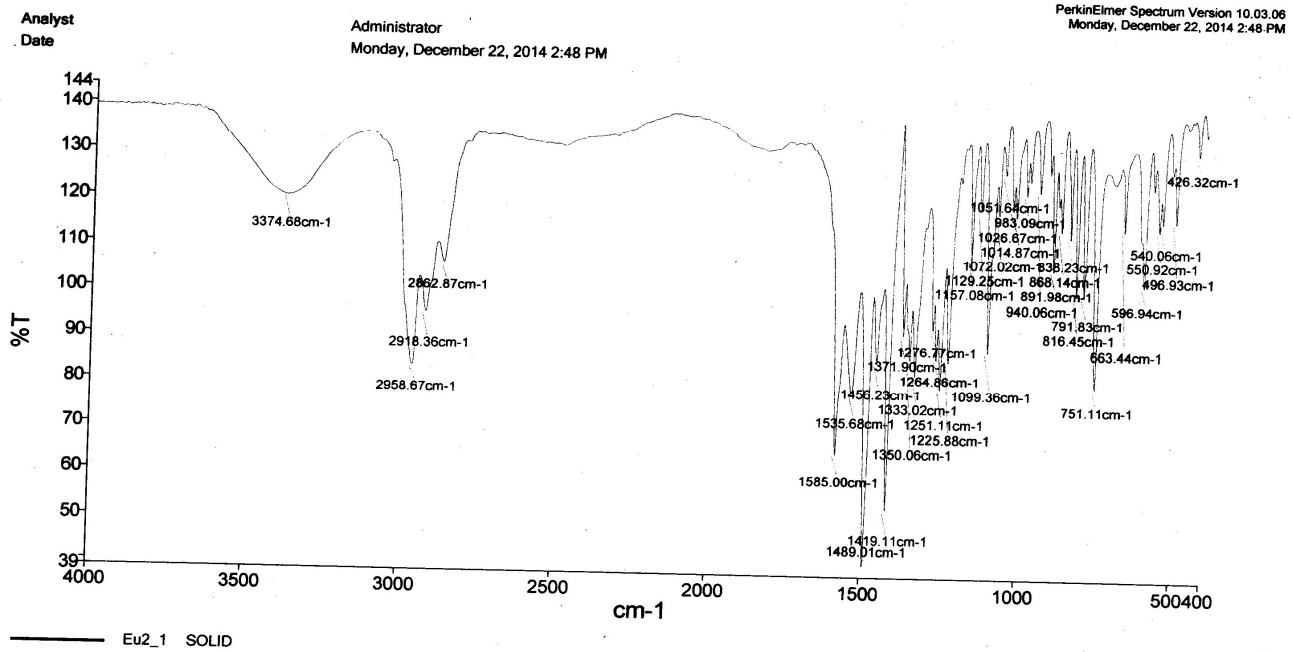

Fig. S23 IR spectra of compound **4** (Eu_2).

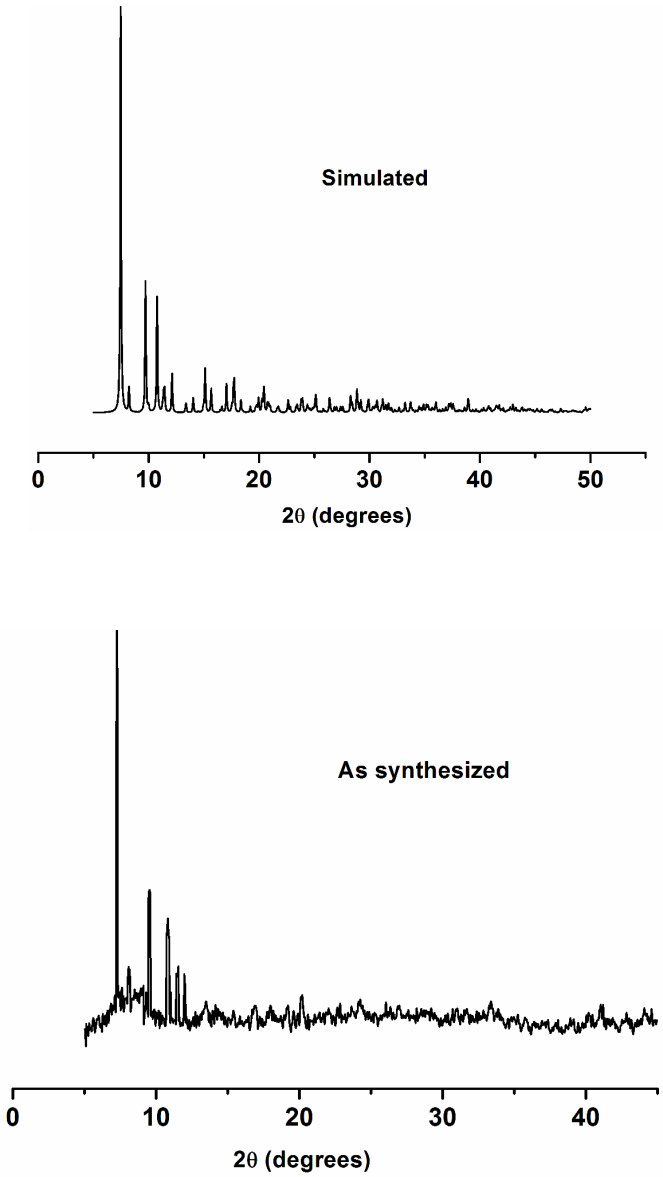

Fig. S24 Room temperature PXRD of compound **1** (Gd_2).

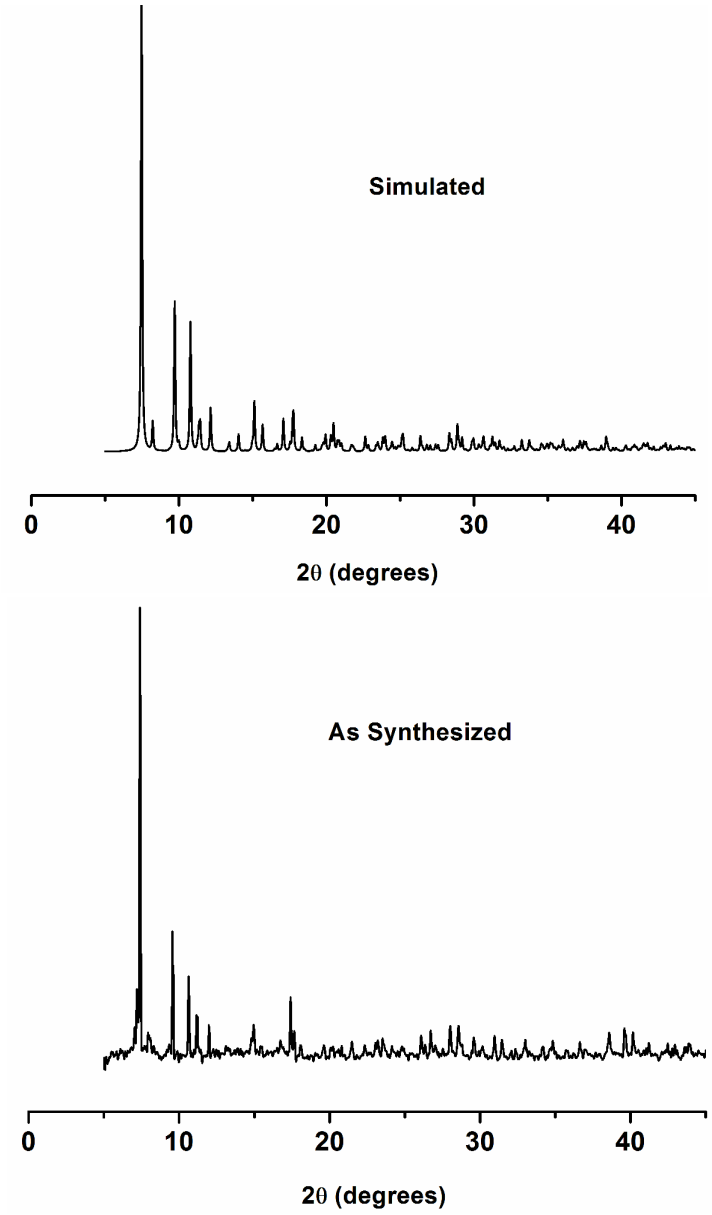

Fig. S25 Room temperature PXRD of compound **2** (Tb_2).

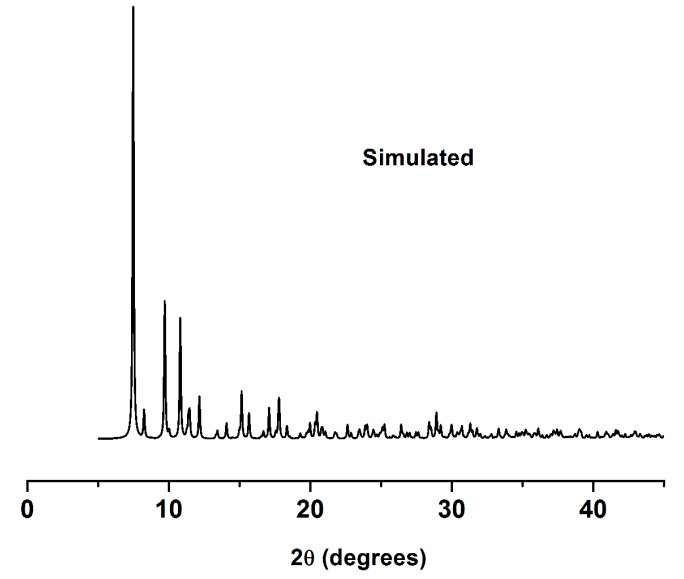

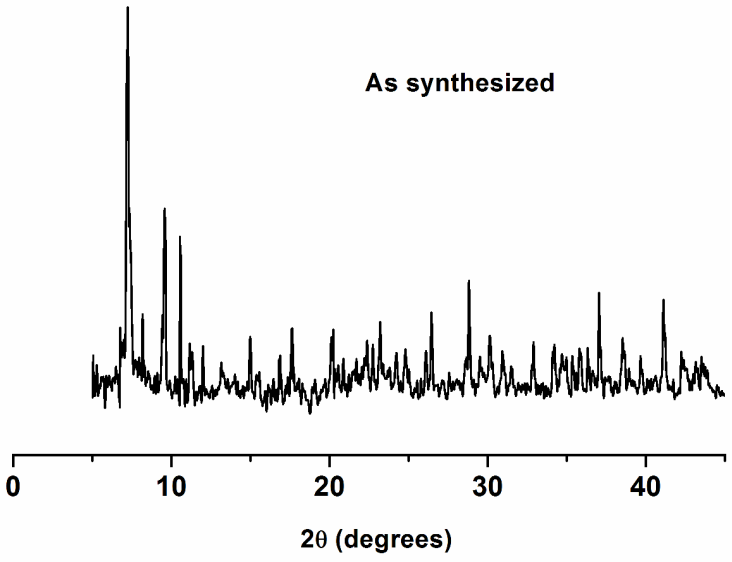

Fig. S26 Room temperature PXRD of compound **3** (Dy_2).

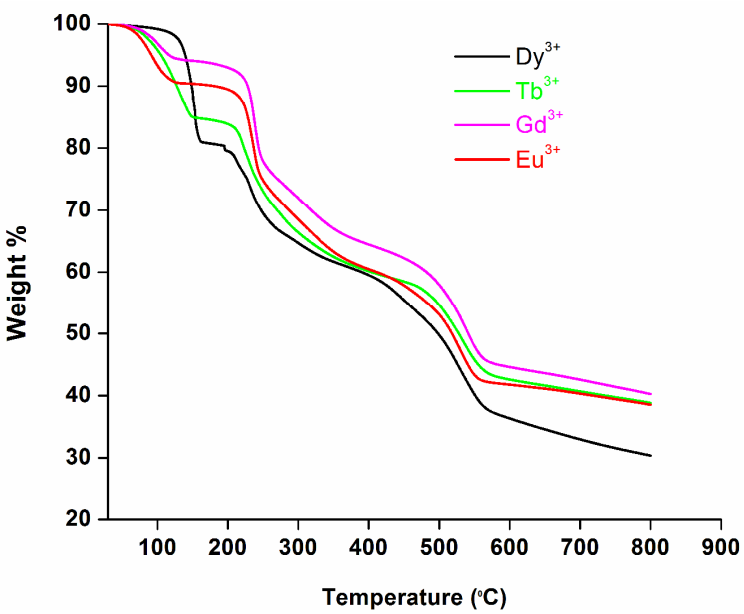

Fig. S27 Thermo gravimetric analysis curve of **1-4** (Heating rate: 10 °C per min) under argon atmosphere.